Union County Solar Energy Awareness

Amanda Pennett '24, Shaunna Barnhart, Ph. D.

Center for Sustainability & the Environment,
Bucknell University, Lewisburg, Pa.

Abstract

Rural communities in Pennsylvania, such as Union County, have a historical and political reliance on traditional fossil fuels like coal, oil and natural gas. Solar energy, an alternative energy source, is a renewable form of energy that is environmentally beneficial to the community, localizes energy production and provides one with energy independence from primarily relying on grid provided electricity. Raising awareness around the potential of solar energy in Union County requires an understanding of the historical view of energy and collection of data on current perspectives around solar to determine the most effective way to communicate its benefits. The path to solar energy looks different for everyone, with residents of Union County facing barriers unique to their state, neighborhood or home. Through survey and interviews, personal challenges and journeys are collected to analyze what tools residents and businesses need to participate in solar energy. Educational materials including a digital infographic and physical brochures that communicate the general benefits, resources and steps to install solar were created for Union County Department of Planning and Development.

Introduction

Solar Energy Expansion

Solar energy has been rapidly expanding across Pennsylvania in recent years as awareness grows as well as local and federal incentives being made available to help finance and make solar energy accessible. With the recent adoption of the C-PACE program in Union County and federal Solar Investment Tax Credits, solar energy in Union County, Pennsylvania has the potential to become widespread and offer energy independence to local residents, businesses and farmers. In order to make an impact on carbon emissions, statewide adoption and awareness of renewable energy is essential, therefore social acceptance in rural communities and counties has become a key aspect in the progression of renewable energy in Pennsylvania.

Solar Energy in Rural Communities

In rural communities, such as Union County, attitudes around solar energy and other renewables can be unique from the average perspective, as the issue of land use as well as the history of coal mining and reliance on oil and natural gas, lead to a variety of strong attitudes towards renewable energy. Examination of Pennsylvania's energy production history, case studies on modern attitudes toward solar energy and the study of federal and local programs and incentives inform the questions that were asked of subjects both in survey and interview. Social acceptance and awareness around solar energy offers environmental, personal and financial benefits that, with widespread adoption, can allow for a reduction in carbon emissions, equity in energy production and energy independence in rural communities.

Methods

This study used a mixed methods approach with a survey including likert scale questions and interviews with local residents.

Survey

Surveys were distributed from July 5-July 26, 2022. A total of 33 respondents from Union County participated in the survey through a convenience sampling method. The survey was distributed across the county at various sampling points to evaluate county residents' general awareness, perspectives, and experiences around solar energy.

It should be noted that while the study attempted to survey and interview across the County, a large portion of the sample came from the Lewisburg area.

Interview

Interviewees were identified through snowball sampling, with a total of 9 interviewees. Interviews of residents with solar and companies who have or attempted to engage in solar energy in Union County shed light on the individual and personal journey to solar energy. Most participants interviewed had solar installed and each participant had a unique path to solar energy and installation preparation.

Results

Several questions were asked pertaining to environmental perspectives and current attitudes around solar energy. 88% of respondents were moderately or extremely concerned about global environmental conditions, and 76% of respondents were moderately or extremely concerned with local environmental conditions.

As shown in **Figure 1**, support for solar is overall strong in most of the common locations and formats. As predicted, utility-scale solar projects garner less support than other, small-scale implementations of solar energy. Another insight, which was not initially predicted, was the lack of support for residential ground-mounted solar installations.

Figure 1.

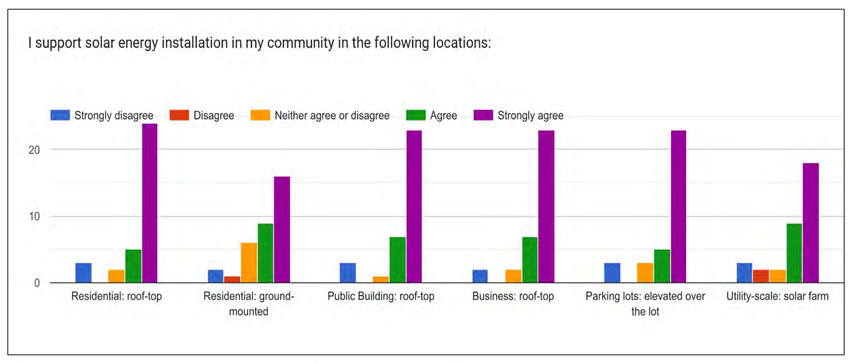

Note: y-axis represents number of responses; n=33

Figure 2.

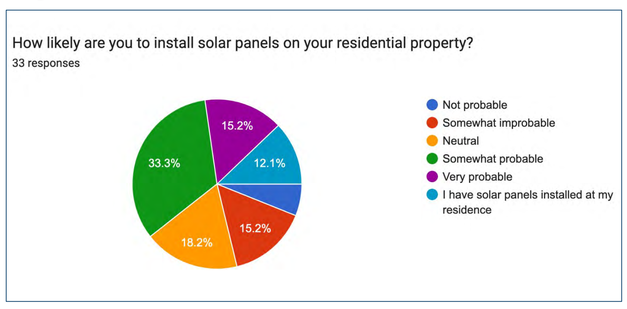

Figure 3.

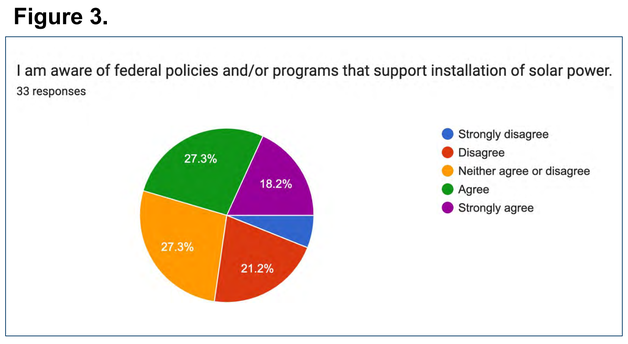

The results are mostly positive in whether respondents believe they would be likely to install solar panels; however, over half of the respondents are either unaware or neutral around federal policies supporting installation of solar energy, and over 70% of respondents are wholly unaware of local policy in support of solar installation. With this considered, county-level policy is limited to the C-PACE program, which was recently adopted by Union County in June 2022. Beyond this, local policy mostly involves zoning regulation of solar installations.

When asked what key factors were most prevalent in keeping Union County residents from participating in solar energy, the most prominent factor was financial concerns, as predicted. Another significant factor shown in **Figure 4** was concerns pertaining to infrastructure. This reflects the nature of many of the homes and buildings in Union County, a rural and historical community. Many either do not have the roof space on their houses or the infrastructure will not be able to support the weight of solar panels.

Figure 4.

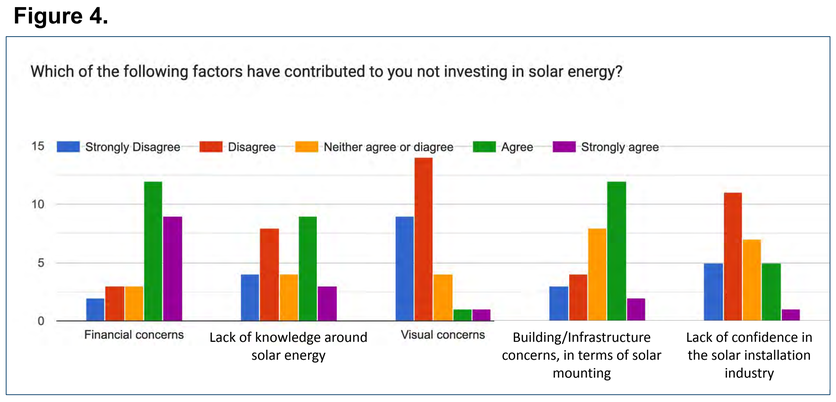

Note: y-axis represents number of responses; n=29

Discussion

Notes on the Survey

The results of the survey reflect a possible motivation to participate in solar energy due to environmental protection and reducing energy consumption. A general unawareness of local and federal policy around solar energy was also shown. While it should be noted that local policy is somewhat limited, this result highlights the need for concise information on the different outlets to adoption of solar energy. It should also be noted that 66.7% of respondents thus far have identified themselves as Democrats, which may have influence on the results.

Reflection on Interviews

Each individual interviewed had a unique journey to how they had accessed solar energy. Many started their participation in solar energy by taking up energy efficiency practices, conserving energy and saving money. The residents with solar installed outlined their motivation as primarily environmental. The business that was interviewed stated the primary motivation for their solar project as economical.

Creation of Educational Materials

The collection of data informed how to communicate benefits and resources around participating in solar energy, to be distributed by the Union County Department of Planning and Development. A working draft of these materials is shown as **Figure 5.** The main pillars to participating in solar energy are outlined so that each resident or business owner can go to whichever point they feel they are at currently. The back page of the infographic includes resources based on the reader's positionality, whether resident, business owner or someone considering a lease.

Figure 5.

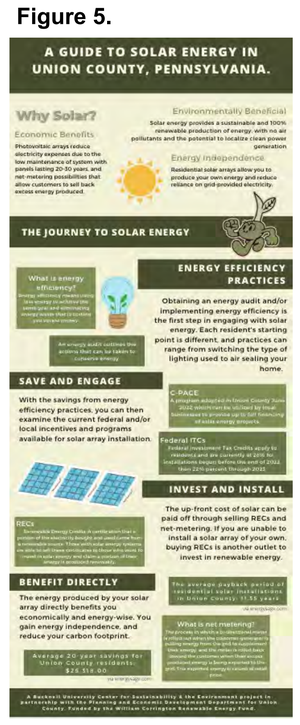

Conclusion

Union County, Pennsylvania, is a rural community that has a long history of reliance on fossil fuels. However, in recent years adoption of renewable energy, including solar, has increased. This expansion can often be limited by a lack of awareness around policy and resources available pertaining to solar energy installment. Through the creation of educational and promotional materials, residents of Union County will have access to information on key programs and benefits of solar energy installation, as shown above in **Figure 5.** Union County residents show a general concern for the environment as well as an interest in solar energy installation, however are unaware of key policies involving solar energy. These materials will work to fill this gap by raising awareness and outlining the path to solar energy.

Acknowledgements

This fellowship project was funded by Bucknell Center for Sustainability & the Environment's William Corrington Renewable Energy Fund.

This fellowship project is in partnership with the Union County Department of Planning and Development.

Thank you to all the participants whether in surveying or through interview.

Opposite Effects of Chronic Stress on Context-Induced Relapse to Palatable Food Seeking after Punishment-Induced Abstinence in Male versus Female Rats

Nicholas Sorkine and Kevin Ball (Faculty Mentor), Dept. of Psychology, Bloomsburg University

Background

Long-term success of dietary treatments for overweight/obesity is low because most individuals relapse to unhealthy eating habits within months of starting treatment [1]. Therefore, investigations into the environmental factors and neural mechanisms that increase one's vulnerability to relapse are critical to the development of novel treatment strategies for obesity, a major public health problem.

Although chronic stress is associated with relapse vulnerability in the clinical literature [2], relatively few pre-clinical studies have used models of relapse that incorporate a chronic stressor. Using classical animal models of relapse, we have shown that exposure to chronic stress increases vulnerability to relapse for at least 1 week after the stress has ended [3-8].

It is noteworthy, however, that in classical animal models of relapse, abstinence is forced by making the reinforcer (i.e., highly palatable, "junk food") unavailable. By contrast, in humans, abstinence is typically self-imposed, despite the availability of unhealthy foods, because the food's rewarding effects are outweighed by the aversive consequences of continued consumption (e.g., obesity-related diseases or stigma). This form of abstinence can be modeled in laboratory animals by punishment of the food self-administration response by response-contingent presentation of mild footshock.

Thus, to increase the translational utility of our findings, we aimed to determine the effects of chronic stress on relapse to palatable food seeking following punishment-induced (self-imposed) abstinence. Given that many of the neurobehavioral consequences of stress are sex dependent, we also aimed to determine whether sex differences exist with regard to the effects of chronic stress on this form of relapse.

Methods

- Phase 1: Self-Administration. Rats were trained to press a lever for highly palatable food reinforcers in daily sessions for 10 days in Context A.
- Phase 2: Punishment + Treatment. Abstinence was achieved in Context B by probabilistic response-contingent mild footshock that gradually increased in intensity over 8 days. Context B was distinct from Context A in its visual and auditory features. After each punishment session, rats were exposed either to daily restraint stress or returned to their home cage.
- Phase 3: Relapse Testing. One week after the last punishment session, rats were tested for relapse in Context A and B (counterbalanced) in the absence of footshock or food.

Results

Males | Females

Change in Body Weight During Chronic Stress

Reinforcers Earned During Punishment Phase

Responding During Relapse Testing in Contexts A and B

Summary and Discussion

- Although chronic restraint appeared to be more stressful in males than in females as indicated by attenuation of weight gain, the effects of stress on punished food self-administration and subsequent context-induced relapse was observed in both sexes.
- Overall, females were more resistant to punishment than males, but restraint caused a decrease in punished food self-administration for both males and females at low shock intensities.
- The magnitude of responding during relapse tests was over 2 times larger in unstressed females compared with unstressed males. Notably, however, a history of chronic stress caused a significant increase in relapse behavior in males, and a significant decrease in females, resulting in similar levels of responding in stressed males and females.
- From a translational perspective, our results suggest that women may be more vulnerable to dietary relapse than men in general, but that exposure to chronic stress confers increased and decreased vulnerability to future relapse in men and women, respectively.
- Such findings should inform the development of sex-specific interventions for dietary relapse and other stress-related

References

Acknowledgements

This [illegible] National [illegible] (DA03[illegible]

Developing an Aversive Stimulus Device using an Arduino

Hannah Needham, Gwen Conley, Dr. James Briggs, Dr. Carl Faust (Advisor)
Susquehanna University

Abstract

To perform behavioral studies, the Susquehanna University psychology department uses a device and associated control program that delivers an aversive stimulus to study fear motivated tasks. The cost of these setups, especially when multiple are required, can be restrictive. The goal is to design an affordable, open-source electronic device for the purpose of psychological behavioral studies using an Arduino. The versatility of the Arduino boards allows for a relatively straightforward circuit to be controlled via code that can be easily understood and modified, as needed, by a user. Key features of a commercial version of the device such as the scrambled sequence and fixed current options are incorporated into our work. Options for improvement of cost and features are discussed.

Device Features

- The program allows for users to input a **desired fixed current (**typical current for this application are 0.1-2mA).
- To calculate the appropriate voltage for each bar the device reads the **equivalent parallel resistance** on each bar.

Figure 1. Equivalent resistance & equation

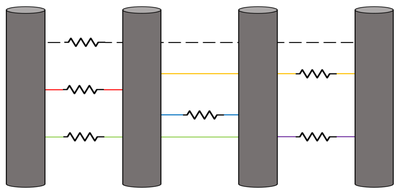

$$\frac{1}{R_1}+\frac{1}{R_2}+\cdots=\frac{1}{R_{eq}}$$

- A **voltage scramble sequence** ensures that the animals cannot miss the stimulus by coincidentally touching bars with like polarity.
- The analog voltage output by the Arduino is produced by pulse-width modulation (PWM). To convert this to a normal analog DC signal a **multi-stage RC filter** is used.
- An **op amp** is used to amplify the filtered voltage signal to ensure that each bar has the voltage required to deliver the desired current value.

Figure 2. Scramble diagram for the grid floor

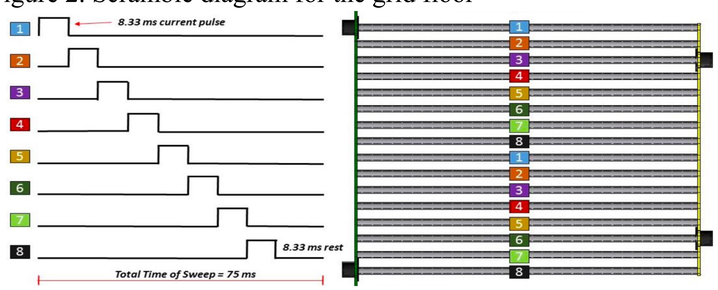

Figure 3. Circuit diagram for a single bar

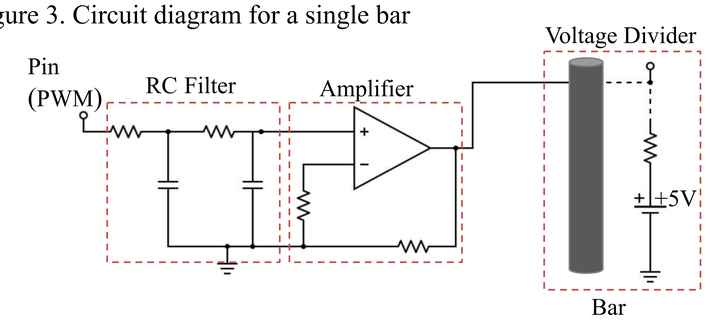

Results

The Hardware:

Figure 4. Circuit for all 8 Bars

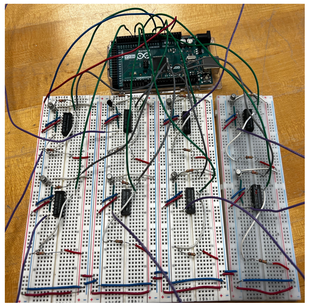

Figure 5. Oscilloscope Scan

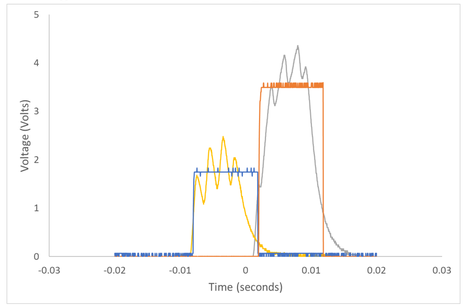

The Program:

Voltage Divider
Relays are activated one at a time to measure the voltage difference across each bar. The program uses a known resistance and the measured voltage to calculate the unknown equivalent resistance across each bar.

Voltage Calculation
From the determine resistances, the program calculates the voltage needed for each bar to deliver the desired current. This value is converted to a number to be used by the Arduino's PWM pins.

Relays
When reading the bar resistance, each relay is activated, in turn. For the following phase, all relays are deactivated and the PWM pins are activated.

Scramble Sequence
The calculated analog voltage is produced by the PWM pin associated with each bar. The program executes the sequence with each bar active for ~8 ms. After each bar receives its pulse, the entire process repeats for a total of approximately 75 ms cycle. The cycle repeats until the desired stimulus time is achieved.

- The program includes adjustable parameters, such as the known resistances, current, number of bars, sequence delay, total current time

Parts/Costs

- Arduino Mega ~$33
- Breadboards ~$3.33/board
- Relays ~$67 for 8, $8.38/relay
- Wire, resistors, transistors, capacitors, op amp
- Grid floor – We used a commercially available grid floor which cost ~$250-300, however a custom-built floor would work equally well for less
- Power supply - to be determined based on final device version

These are initial parts; further cost reduction is possible

Discussion & Conclusion

- Status of work shows that device can reproduce the following features
  - Scramble sequence
  - Resistance readings
  - Voltage adjustment
- Adjustments to the amplifier portion will be needed to reach voltages necessary to produce desired currents.

Future Work

- A button should be added so the program only must run for as long as the button is pressed for.
- To create a more compact electronic, the elements should be transferred to a PCB and enclosed.
- The program and electronic is currently set up to execute the 8-pole mode, but the program could be altered to execute the 2-pole mode.
- Add in other desired stimulus features, including lights, tones, and cameras.

References

- *Model H13-15 Precision Shock Generator Scrambled, 8-Pole Output Mode.* [Online]. Available: https://www.harvardapparatus.com/media/manuals/Product%20Manuals/H13-15%20Working%20Procedure%20with%20Shock%20Floor%20and%20Voltmeter.pdf

Susquehanna UNIVERSITY

Precision 3D Modeling

Amanda McLaughlin and Adam Hansell, PhD.
Susquehanna University

Abstract

The physics department at Susquehanna University has recently procured a collection of 3D printers for use by the students. However, many students and faculty as well do not have a complete understanding of the inner workings of the machinery, and the programs to create a printable model. My work is to understand and relay, in the form of simple cohesive directions, a general understanding of how to create and print a model. The aim of this research is to create a guide that after reading an individual can create from start to finish a model of their creation.

Filament vs. Resin

Within the realm of 3D printing there is many different types of materials that can be printed. In this we will discuss filament, a type of plastic with a relatively low melting point, and plastic resin, which is melted with UV light.

- Fused Deposition modeling (FDM: In most cases discussed here we will be using PLA filament which stands for Polylactic Acid it is a 100% bio sourced plastic.
  - Most common for starting 3D printing
  - Easy to use and warp issues
  - Environmental stances

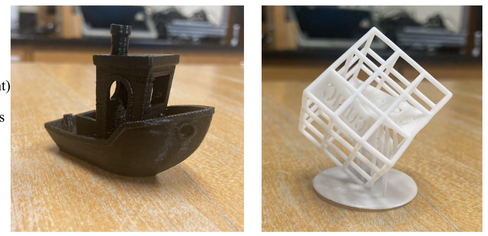

Figure-1: A FDM (left) and resin (right) print that show the possible difficulties each printer may run into

- Resin: Though FDM printing has many structural abilities then resin we see that resin printing is still used quite often.
  - Coherent designs come out perfectly
  - High accuracy
- However, we don't see resin printers outweighing filament.
  - Cost
  - Structural integrity
  - Ease of use process

Modeling programs

There are many ways in which a user can create a model with which to print. Here outlined is three of the common interfaces along with their success and drawbacks.

- Tinkercad
  - Online program
  - Simple interface
  - Shapes and colors
- Sketchup
  - Online program
  - Coordinate system base
  - Drawing interface
- Autocad
  - Downloadable program
  - Free space interface
  - Intricate design format

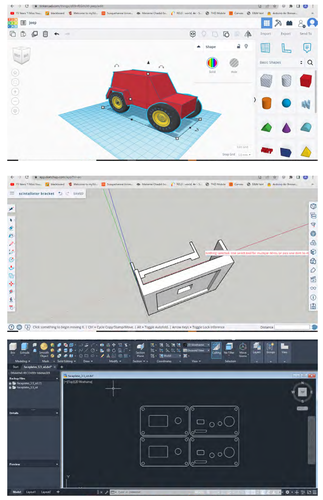

Figure-2 :three different possible modeling systems. Tinker cad (top), Sketchup (middle), Autocad (bottom)

Each of these programs have their own specific uses. For a beginner or younger user Tinkercad would be a fantastic start, but for an intermediate user not looking for highly intricate plans Sketchup would be the best decision. Autocad would be used for those looking for a program that has a wide range of uses, and is highly intricate, but not necessarily intuitive.

Slicing

After creating a desirable model, one cannot simply upload that to a printer and print it out. To print a 3D model you created you must put it into a slicing software. Slicing is the process in which a program turns a 3D model into instruction for a 3D printer

In this research I primarily used two types of slicing software:

- Cura
  - FDM printer based
  - Free program
  - Custom vs. recommended options
- Photon Workshop
  - Given with anycubic printer
  - Specifically for resin

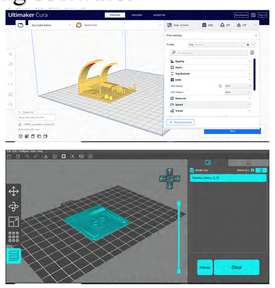

Figure-3: Slicing programs Cura (top) and Photon workshop (bottom)

Calibration

Calibration is a very prominent part of printer set up, but in actuality calibration is used throughout the whole lifespan of a printer. Due to unforeseen changes a printer that was calibrated when set up can suddenly have difficulties printing very simple products

- FDM Printer
  - Leveling
  - Z-offset
  - Temperature/pre-heating
- Anycubic resin printer
  - Z-offset
  - Exposure time

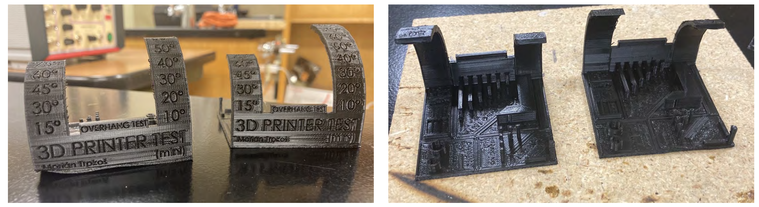

Figure-4: Two printer tests printed before and after calibration

Future work

This whole project started because of a simple box needing to be printed, and now after making sure that those were all precisely printed I found myself with a need for more understanding.

My goal for this project is to create a manual that a person can use to from nothing print a model of their own creation. I have run into quite a few issues on the way that I still need to know how to trouble shoot, but this is an ongoing project that Susquehanna University can use for many years to come

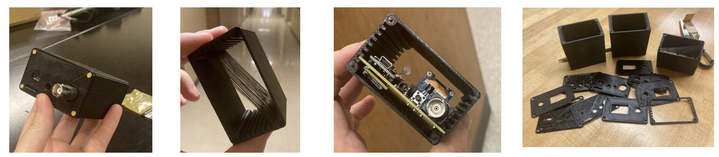

Figure-5: Different printed models and the failures. Final product (left most)

Susquehanna UNIVERSITY

Visualizing Acid Mine Drainage in the Shamokin Creek Watershed: Environmental Injustices and Consequences from Coal Mining

Benjamin Shimer ‘24, Shaunna Barnhart PhD
Bucknell Center for Sustainability & the Environment
Bucknell University, Lewisburg, Pa.

Abstract

Coal mining has been a prevalent aspect of life in the 13 state Appalachian region, including Pennsylvania. Towns built around the industry enjoyed economic benefits until resource exhaustion and other market factors interfered, resulting in coal mines being abandoned with profound economic, social, and environmental impacts for the communities around them. In the City of Shamokin, this negligence led to economic downturn and environmental consequences such as acid mine drainage. Through work with the Shamokin Creek Restoration Alliance, maps were constructed to visualize the characteristics of acid mine drainage in the watershed and observe the relationship between AMD and socioeconomic data. GIS mapping helped convey the environmental injustices endured by a region with comparatively high poverty and disability rates, many vacancies, low educational attainment, and low income, while providing data that could be useful for planning treatment processes for acid mine drainage.

Mining History

Since the industrial revolution, fossil fuel extraction has been a prominent force impacting the economy, quality of life, and environment of the communities attached to these industries. Rich mineral deposits in the Appalachian mountains encouraged extraction processes that impacted the economy and environment of the region for centuries (Morrone et al 2011). The creation and abandonment of coal boomtowns left environmental degradation and vacated buildings as the industry’s lasting trace (White 2013).

The combined legacy environmental, social, and economic factors create an environmental justice issue for coal towns. Studies have shown statistically significant relationships between one’s residence in a coal-mining county and poor self-reported health, relationships that only grow more conclusive when specifying residence in an Appalachian coal-mining county (Zullig 2010). In addition, these Appalachia counties have historically had higher poverty rates, lower per capita incomes, and less education compared to national averages (arc.gov).

The City of Shamokin is one such place in the region that has endured the highs and lows of coal mining. Once a prosperous anthracite coal mining town, Shamokin, along with the adjacent Coal Township, experienced economic growth from the industries of coal mines and silk mills, however this did not last. The great depression, market shifts to oil and cheaper synthetic textiles, and the loss of Shamokin’s two railroads led to a decrease in Shamokin and Coal Township combined population from 50,000 at its peak to around 18,000 now (shamokincity.org).

Figure 1: Historic postcard of the Glenburn Colliery. Source: wynninghistory.com

Acid Mine Drainage

Acid mine drainage (AMD) is a chemical process that occurs when water running through underground mine shafts, mine waste dumps, tailings, open pits, and/or ore stockpiles interacts with pyrite and oxygen to form ferrous oxide and sulfuric acid (Moeng 2017).

$$4FeS2(s)+15O2(aq)+14H2O(aq) \rightarrow 8H2SO4(aq)+4Fe(OH)3(s)$$

Ferrous oxide is commonly referred to as “yellow boy” for its distinguishable color, while sulfuric acid decreases the pH of the water, making it highly acidic.

Photo taken by Benjamin Shimer

Photo obtained from shamokincreek.org

When pH levels decrease to below 5.5, severe consequences for biotic communities ensue, effectively making the water uninhabitable for species such as trout. In addition, low pH levels can inhibit plants from receiving necessary nutrients by immobilizing nitrogen, phosphorus, and potassium while creating deficient levels of calcium and magnesium (Rodriguez-Galan 2019). Instead, it increases the presence of dissolved heavy metals including iron, aluminum, manganese, and sulfate which can be severely detrimental to water quality (Moeng 2017, Rodriguez-Galan 2019). These metals also have significant consequences on aquatic life and plant growth (AMRClearinghouse).

Shamokin Creek Restoration Alliance

The Shamokin Creek Restoration Alliance is a dedicated group of volunteers working to address acid mine drainage in the Shamokin Creek Watershed. The maps created around the subjects of environmental justice and AMD remediation serve to aid them in grant proposals and will be featured on their website to visualize the socioeconomic and environmental complications they have worked hard to ameliorate over the past 25 years.

Maps

Shamokin Creek Watershed and AMD Overview

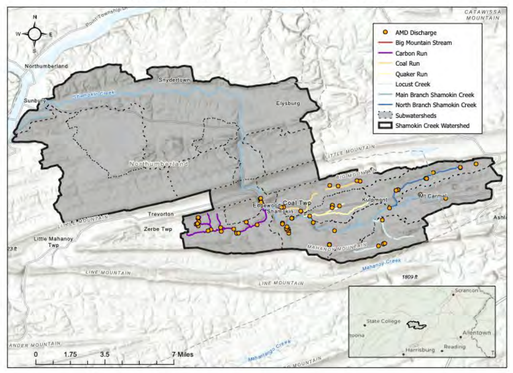

Disability in the Lower Shamokin Creek Watershed by Block Group

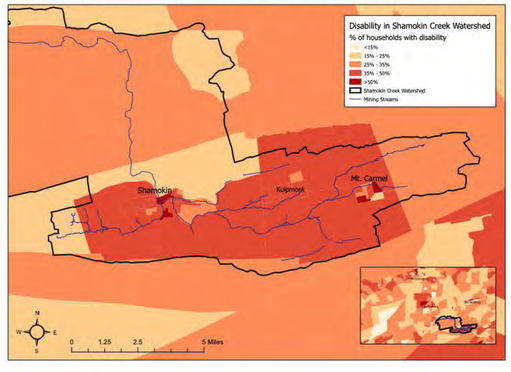

Shamokin Creek Watershed High Baseflow AMD Flow Rate

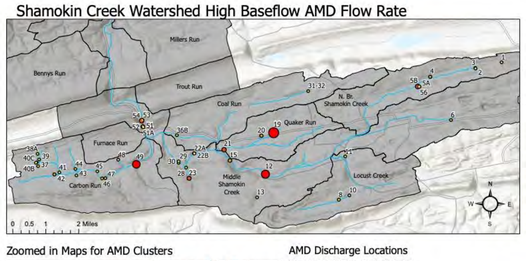

Zoomed in Maps for AMD Clusters

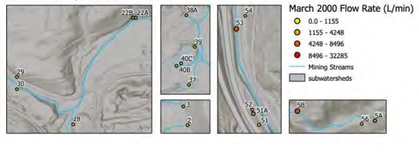

AMD Discharge Locations
March 2000 Flow Rate (L/min)
0.0 - 1155
1155 - 4248
4248 - 8496
8496 - 32285
Mining Streams
subwatersheds

Data Collection

Water quality data for the maps were provided through Cravotta and Kirby’s 2004-05 USGS report on the Shamokin Creek Watershed. The 2019-2020 US Census Data from the American Community Survey and existing map layers from Dr. Carl Kirby, PASDA, and Northumberland County were also used in this work.

Discussion

GIS visualization of AMD in the Shamokin Creek Watershed highlights points of significant and harmful water chemistries immediately. Through the variations of color and size of discharge locations, the viewer of each AMD discharge map can quickly gather which sites have high iron concentrations, high flow rates, low pH, or other listed consequences of AMD depending on the map presented. This data is important for designing treatment plans and understanding the severity of each discharge.

The socioeconomic maps show the AMD impaired watershed to be more vulnerable to environmental inequality. Rates of disability and poverty are high with disability in Shamokin being nearly twice that of the PA average, and poverty rates being triple the PA average. Median income is reported to be half the statewide numbers, and educational attainment in Shamokin and the surrounding areas has also been identifiably low through the displays. The relationship between environmental degradation and social/economic inequality is made visible through the series of maps depicting AMD and census data in the Shamokin Creek Watershed

Acknowledgements

I would like to send thanks to those apart of the Katherine Mabis McKenna Foundation Summer Environmental Internship for funding and support of this project, Dr. Shaunna Barnhart of the Bucknell Center for Sustainability & the Environment for her mentorship, Dr. Carl Kirby for sharing his extensive knowledge on AMD in the Shamokin Creek Watershed, Bucknell GIS specialist Janine Glathar for her technical support, as well as SCRA members Steve Motyka, John Buccanelli, and Heather Makal for their active involvement and support.

References

1. *AMRClearinghouse.org. (*n.d.). Retrieved June 23, 2022, from http://www.amrclearinghouse.org/
2. *About the Appalachian Region*. (n.d.). Appalachian Regional Commission. Retrieved June 21, 2022, from https://www.arc.gov/about-the-appalachian-region/
3. Moeng, K. (2019). *Community perceptions on the health risks of acid mine drainage: The environmental justice struggles of communities near mining fields.* Environment, Development and Sustainability, 21(6), 2619–2640.
4. Morrone, M., Buckley, G. L., Davis, D. E., & Purdy, J. (2011). Mountains of Injustice: Social and Environmental Justice in Appalachia. Ohio University Press.
5. Rodríguez-Galán, M., Baena-Moreno, F. M., Vázquez, S., Arroyo-Torralvo, F., Vilches, L. F., & Zhang, Z. (2019). Remediation of acid mine drainage. Environmental Chemistry Letters, 17(4), 1529–1538.
6. History of the City of Shamokin. (n.d.). Retrieved July 19, 2022, from http://www.shamokincity.org/history.htm

Using Smartphone GPS Data to Analyze Athlete Performance

Students: Brandon Burkett (Computer Science & Engineering ‘23)
Faculty/Staff mentors: M. Stu Thompson (Electrical and Computer Engineering)

Bucknell UNIVERSITY

Background

The long-term objective of this project is to improve wellness and track the performance of student-athletes by monitoring their real-time quantitative movement data.

Driving Questions:
- How can smartphone GPS data be used to analyze athlete performance?
- How does smartphone GPS data compare to more expensive solutions?
- Is the smartphone data reliable?
- How do we quantify “good” vs “bad” data?

Methods

- 6 Android phones and 6 iPhones were carried together
- Phones were turned on and allowed to warm up
- Four laps were made around the field (Figure 1)
- Start/end time was recorded for each session
- Apps recorded longitude/latitude data
- 13 sessions completed over 30 days
- Baseline location data was collected with survey-quality equipment
- Session results compared with the baseline location data

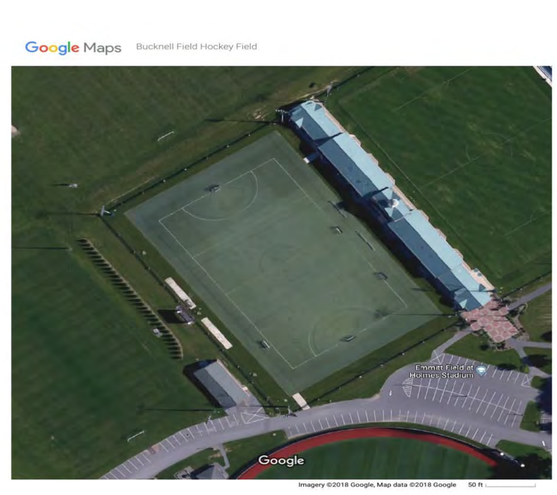

Figure 1: Bucknell Field Hockey Field

Results

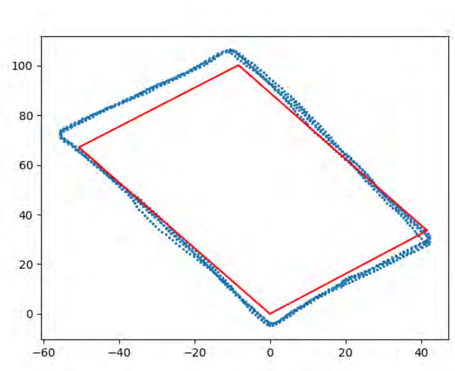

Figure 2: A “Good” Plot
NEXUS5X-01 07/30/2021 Longitude/Latitude

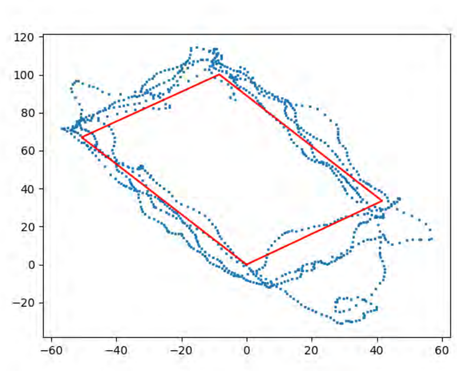

Figure 3: A “Bad” Plot
IPHONE8-02 08/03/2021 Longitude/Latitude

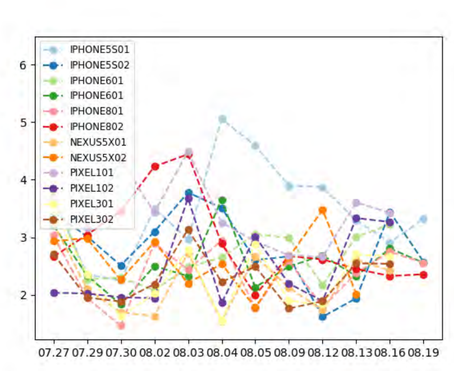

Figure 4: Device Plot
Mean Error Distance for each Device (m)

	IPHONE5S-01	IPHONE5S-02	IPHONE6-01	IPHONE6-02	IPHONE8-01	IPHONE8-02	PIXEL3-01	PIXEL3-02	PIXEL1-01	PIXEL1-02	NEXUS5X-01	NEXUS5X-02	Daily Mean
7.27	1190.340749	1209.578557	1212.287198		1244.005721	1254.305638	1238.258037	1207.129219		1220.268577	1209.569958	1182.679047	1216.84227
7.29	1294.599882	1287.298025	1216.248277	1182.513195	1203.408288	1344.210202	1199.598444	1215.295717	1104.712961	1185.622152	1198.294063	1206.267181	1219.839032
7.3	1249.375983	1311.340819	1200.9712	1189.415589	1200.930658	1376.964844	1195.001248	1220.001279	1122.084833	1235.338801	1189.467483	1196.32065	1223.934449
8.02	1219.792281	1269.369975	1149.927354	1200.808114	1233.761613	1271.946646							1224.267664
8.03	1392.917647	1265.669102	1205.312519	1197.73342	1278.279728	1515.792971	1205.025721	1200.687385	1118.06131	1245.114273	1197.640263		1256.566758
8.04	1667.85347	1401.045831	1159.059139	1315.876265	1390.731322	1236.23704	1198.642072	1219.91419	1092.35822	1182.170512	1195.636969	1189.648376	1270.76445
8.05	1520.7701	1270.9151	1366.248588	1187.789244	1241.540013	1220.777167	1205.657587	1232.105263	1175.907629	1228.967267	1200.799345	1193.372608	1253.737493
8.09		1196.854532		1171.957486	1211.144098	1197.645626	1201.990103	1151.610675	1126.462474	1154.109942	1191.952962	1170.637117	1177.436502
8.12	1291.17787	1196.282673	1058.082181	1203.072923	1216.641872	1261.292565	1229.429015	1257.112314	1099.467041	1179.118456	1185.611803	1190.925169	1197.351157
8.13	1236.730251	1178.516132	1168.125187	1240.358092	1315.323122	1332.790721	1201.150194	1222.453075	1136.239793	1170.773368	1206.472093	1171.953143	1215.073764
8.16	1269.915299	1288.321399	1246.153682	1199.486974	1217.295184	1236.892857	1227.892023	1239.425971	1122.142654	1205.986013	1175.472371	1192.425092	1218.450793
8.19	1239.795505	1237.711616	1191.673832	1192.921345	1211.124031	1229.665607	1212.646497	1211.266175	1108.471596	1191.075574	1197.684332	1190.628199	1201.222026
8.26	1183.061248	1255.922933	1144.512188	1174.450977	1210.957206	1215.287801	1191.366739	1189.035195	1096.711748	1217.509754	1198.912666	1252.196633	1194.160424
Max-Min	484.7922217	222.5296989	308.1664068	143.9187784	189.8006643	318.1473452	46.89129845	105.5016397	83.5494093	91.00433047	34.09758646	81.55951543	

Figure 5: Total Distance Traveled (m)
Darker cells are furthest from the actual measured distance of 1171.2m

	IPHONE5S-01	IPHONE5S-02	IPHONE6-01	IPHONE6-02	IPHONE8-01	IPHONE8-02	PIXEL3-01	PIXEL3-02	PIXEL1-01	PIXEL1-02	NEXUS5X-01	NEXUS5X-02	Daily Mean
7.27	1.999454644	1.812700468	3.157666091	1.526446298	1.898706695	1.847880403	2.238843717	1.732582773	5.058746491	2.321348383	1.628944101	1.272772208	2.208007689
7.29	2.148634174	1.945618353	1.669249595	1.172514899	1.237987152	2.082084724	2.187602107	1.708454202	1.916430111	1.576193707	1.388902022	1.488371346	1.710170199
7.3	3.327638577	3.188651703	1.770360857	1.391603493	2.462237563	3.820368263	1.513259239	1.668549199	4.447089754	1.975558946	1.277933525	1.47104038	2.359524292
8.02	2.42489849	2.025501432	1.3123063	0.9376423172	1.417377695	2.547993163							1.777619899
8.03	2.596270201	2.997197945	1.932620361	1.105964501	1.725348523	4.428750726	2.298349942	1.377101821	4.264665859	2.151305743	1.926017516		2.436690285
8.04	5.300844409	2.873543304	1.324520202		2.077177888	1.938615835	1.221713484	1.539029134	2.454908271	2.462465883	1.339759472	1.485669757	2.183477058
8.05	4.394514115	2.922152915	3.294106069	1.277582471	2.185122348	1.943378265	1.854793609	2.23510645	3.008908784	1.894554906	2.011526247	0.958715532	2.331705143
8.09	3.395572679	1.344246769		1.417407608	1.387467854	1.00579238	1.747090791	2.487171167	2.795711682	2.153993401	1.06663472	0.9078861174	1.791725015
8.12	3.647414497	2.676141611	3.37280853	1.308281342	1.742265461	2.105691578	2.284050404	2.445764713	2.271535412	3.091880341	1.495861852	1.770501126	2.351016405
8.13	3.529015059	2.04988453	1.786576613	1.679254366	3.599452927	3.15688267	1.592540826	2.124293885	2.572267628	2.298006419	2.155677414	1.296386506	2.320019904
8.16	3.737229644	2.437529993	1.787115106	1.075538133	1.499360193	1.555510332	2.471754152	1.553386284	4.239034544	1.853918317	1.133969888	1.481032649	2.068781603
8.19	4.278207179	2.487669306	1.399336047	1.328683852	1.443336798	1.662723318	2.078629651	1.78810941	2.95382333	2.092022034	1.705962755	2.075282364	2.107815504
8.26	2.779620722	2.936982803	1.2308538	1.006461573	2.597406634	1.251386225	2.367626127	1.927749312	2.391633162	1.889779932	1.175941728	1.715008831	1.939204237
Max-Min	3.301389765	1.844404934	2.141954729	0.7416120484	2.361465775	3.422958346	1.250040668	1.110069346	3.14231638	1.515686633	1.089042694	1.167396247	

Figure 6: Mean Error (Point to Line) Distance (m)
Darker cells are further from a Mean Error Distance of 0m

Conclusion

Through our findings, we can see that there is no clear reason for the chaotic nature of certain devices.
Going forward, we want to explore other statistical measures to quantify the data. We want to see if the location on the field affects the accuracy of the data. We also want to explore

References

Acknowledgements

- ECE department & College of Engineering
- Jason Forsyth at JMU

Leveraging Ovis Canadensis Horn Shapes for Impact Mitigation

Jacob M. Schaefer[1], Benjamin B. Wheatley[2]

[1]*Department of Mechanical Engineering, Bucknell University, Lewisburg PA*

[2]*Department of Mechanical Engineering, Bucknell University, Lewisburg PA*

Mechanics and Modeling of Orthopaedic Tissues Lab

Bucknell University

Introduction

- Bighorn Sheep (Fig. 1) ram heads repeatedly during mating season and accumulate low amounts of trauma
- After impact, the horn tips oscillate medial-laterally, which reduces brain cavity accelerations [2]
- Traumatic brain injuries (TBI) in humans occur frequently

Figure 1. Ovis Canadensis or Bighorn Sheep [1].

Goal: Determine the extent that horn-like shapes can reduce accelerations after impact.

Methods

- Create ram horn impactor designs (Fig. 2A) in Solidworks
- Export into finite element software (Abaqus) for meshing and analysis
- Simulate dynamic drop test experiment (Fig. 2B) using explicit finite element solver
- The acceleration data will be compared across simulations with different geometries

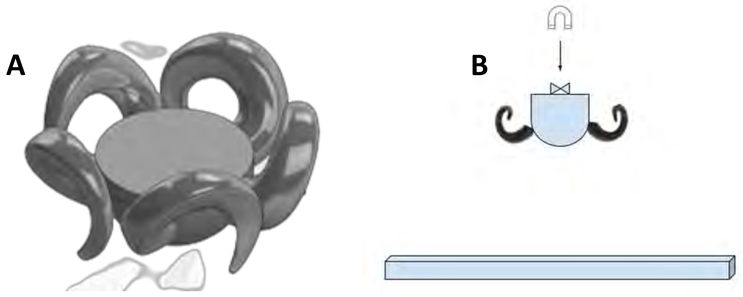

Figure 2. A) 5 Horn impactor geometry. **B)** Drop test design.

Results

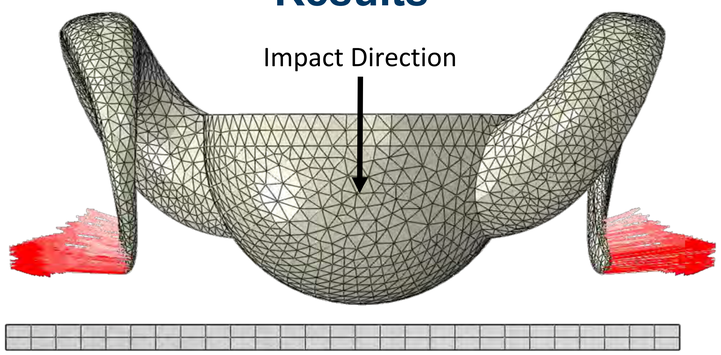

Figure 3. Vector plot of two horn impactor shape measuring velocity.

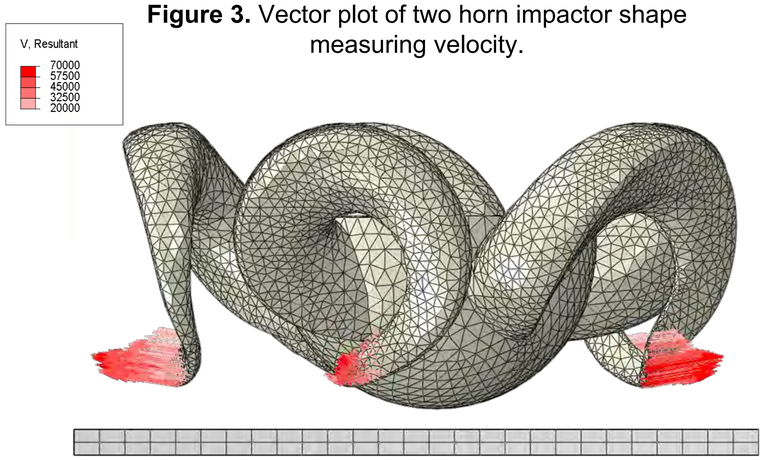

Figure 4. Vector plot of a five horn impactor shape measuring the magnitude of velocity.

	2 Horns	5 Horns
Max Acceleration in Vertical Direction (m/s^2)	**8936**	**8163**
Max Velocity of the Horn Tips (m/s)	**71.9**	**64.9**

- There exists medial-lateral velocity seen at horn tips after a drop (Fig. 3).
- Energy is required to facilitate the oscillates of the horn tips
- Relative to the impact velocity, the horn tips oscillate at high velocities (Fig. 4).

Discussion

- As the number of horns (and thus oscillations) increases, the max acceleration tends to decrease
- Reducing max accelerations to the brain cavity also reduces the likelihood of a TBI
- There exists a need to verify simulated results with real testing
- Horn tips oscillate perpendicular to direction of impact, reducing acceleration in brain cavity

Future Work

Figure 5. 3D printed 2 horn-impactor geometry and its corresponding silicone cast.

- Experimental drop test will be completed using silicone castings of 3D printed geometries (Fig. 5)
- Acceleration will be measured with high-speed imaging and accelerometers and compared across different geometries following drop test
- Acceleration data/observations from real drop test will be used to verify the modeling results

Acknowledgements and References

Authors would like to acknowledge the Costa Healthcare Fund at Bucknell University for support.

[1] *Bighorn Sheep*. (2007). [Photograph]. The National Wildlife Federation.

[2] Drake, A et al. *Acta Biomaterialia 2016.* doi: 10.1016/j.actbio.2016.08.019

The Role of *Dm* Ime4 in *Drosophila melanogaster Spermatogenesis*

Mary Kuziak, Savannah Barton, Rosemarie Mirabella, and Dr. Antonio Rockwell
Susquehanna University

Introduction

N6-methyladenosine (m6A) is the post-transcriptional methylation of RNA at the N6 position of adenosine and is involved in both physiological and pathological functioning of eukaryotes. m6A has been associated with a multitude of cancers and viruses and is essential in RNA splicing and translation[1]. There are multiple proteins that play a role in the m6A modification mechanism that are essential to its function, such as *Dm* Ime4. *Dm ime4* is a gene that encodes the enzyme that is necessary for m6A to occur. Previous research suggests that *Dm* ime4 is localized in the gonads in *Drosophila*. In *Drosophila* testes *Dm* ime4 deficiency leads to germline cell death[3]. The phenotype of a swollen tip was also observed in *Dm* ime4 deficient mutants, this unique phenotype was also seen in Tudor-SN (TSN) mutants[2,3]. TSN is a protein that participates in multiple molecular functions and has been shown to be required for transposon silencing[2]. Due to observed phenotypic similarities in *tsn* and *Dm ime4* mutants, our lab is conducting research to determine if TSN is regulated by *Dm* Ime4.

The importance of Spermatogenesis as a model:
Our lab is studying the potential regulation of *tsn* in *Dm ime4* in spermatogenesis. Germline cells undergo multiple cycles of mitosis and meiosis to create spermatids. These spermatids then elongate and mature into sperm[4]. Spermatogenesis is a well understood and recognized mechanism, thus making it an ideal model for observing abnormalities. Testes are also clear, making immunostaining especially useful. Since spermatogenesis goes through both mitosis and meiosis, abnormalities that are observed in these systems can be applicable to other cells that undergo mitosis (somatic) and meiosis (gamete).

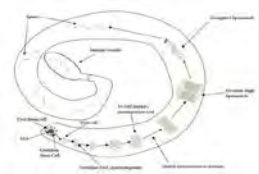

Figure 1. During spermatogenesis a germline cyst cell, which is contained within two somatic cyst cells, undergoes four cycles of mitosis and two cycles of meiosis. This process forms 64 spermatids that are bundled together which mature to become sperm.

Methods

Drosophila Strain: Ime4^{c1}/TM3^{sb} generated via P element mutagenesis.
Immunostaining: Testes were dissected from progeny and fixed and permeabilized for staining. DAPI was applied to detect spermatid bundle numbers.
Confocal Imaging: Testes images were obtained from prepared slides using Nikon 700 confocal microscopy.

Results

Figure 2. A segment of the TSN gene sequence with *Dm* Ime4 binding sites, AAACC highlighted yellow and AAACA highlighted green. The most probable hairpin structure RNA sequences are bolded for each binding site.

Figure 3. Most likely AAACC *Dm* Ime4 binding site RNA hairpin structure for TSN with the amount of energy used. Generated using University of Rochester RNA structure prediction database.

Figure 4. AAACA *Dm* Ime4 RNA sequence binding site for TSN that forms a secondary hairpin structure with the amount of energy used. The figure was generated using University of Rochester RNA structure prediction database.

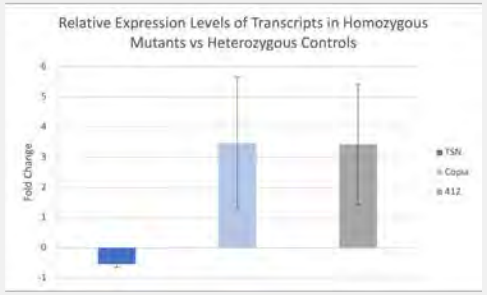

Figure 5. Average fold change quantified using RT-qPCR for TSN, Copia, and 412. TSN is associated with the regulation in transposons where a decrease in expression shows an upregulation in the transposons Copia and 412 due to deficiency in *Dm* Ime4.

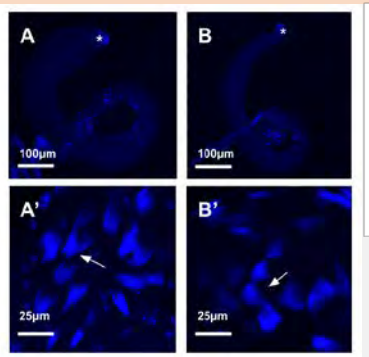

Figure 6. Spermatid bundle localization for whole and tail of testes. Confocal images with DAPI stain. A-A': 16FRT/16FRT. B-B':16FRT/Tm3^{sb}. Arrow points to a spermatid bundle.

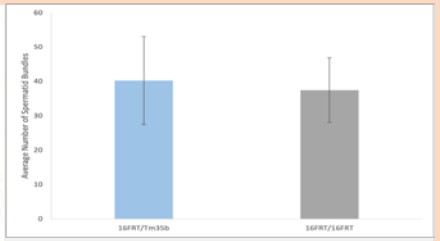

Figure 7. Average number of spermatid bundles counted for 16FRT/Tm3^{sb} and 16FRT/16FRT. No difference was observed thus far in our research. (p-value: 0.8)

Conclusion

Dm ime4 is a gene essential for development in Drosophila and the process of spermatogenesis. Aspects such as binding sites, energetically favorable hairpin structures, and the significant decrease in TSN with upregulation of transposons in mutants are all evidence of a conserved mechanism where *Dm* ime4 regulates TSN. Spermatid bundles are quantified to show the regulation of transposons with TSN. It can be expected that due to the deficiency of TSN there would be a decrease in spermatid bundles, however, there was no significant difference observed in the limited amount of research conducted thus far. Overall, our research suggests that there is a potential connection between TSN and *Dm* ime4. If conserved, this research can offer prospective translational research opportunities.

References

1. Jiang, X., Liu, B., Nie, Z. et al. The role of m6A modification in the biological functions and diseases. Sig Transduct Target Ther 6, 74 (2021). https://doi.org/10.1038/s41392-020-00450-x
2. Ku H-Y, Gangaraju V. K., Qi H, Liu N, Lin H (2016) "Tudor-SN Interacts with Piwi Antagonistically in Regulating Spermatogenesis but Synergistically in Silencing Transposons in Drosophila." *PLoS Genet*, vol. 12. https:// doi.org/10.1371/journal.pgen.1005813
3. Rockwell, A. L. & Hongay, C.F. (2020). "*Dm* Ime4 depletion affects permeability barrier and chic function on drosophila spermatogenesis". *Mechanisms of Development*, vol. 164. https://doi.org/10.1016/j.mod.2020.103650.
4. Rowe, L. & Rockwell, A. L. (2022). Ubiquitous Knockdown of Mettl3 using TRiP.GL01126 Results in Spermatid Mislocalization During Drosophila Spermatogenesis. *MicroPubl Biol*. 10.17912/micropub.biology.

Building a Digital Twin: A Virtual Model of an Electric Vehicle

Hannah Kim
Bucknell University
Department of Mechanical Engineering, Bucknell University, Lewisburg, Pa.

Introduction

Summer Research Objectives

- Create a digital twin for the P1 Electric Vehicle using Simulink
  - Using Arduino (microcontroller) as an interface for the code
- Gain understanding of basic electronics and vehicle dynamics
- Improve problem solving skills and deepen appreciation for learning

P1 Electric Vehicle

- A student-built electric drive-by-wire vehicle owned and operated by Bucknell University.
- Has been used for many research investigations: stabilization at the limits of handling, lane-keeping assistance, road friction and state estimation

What is a Digital Twin?

Digital Twin vs. Simulation

- Complex System vs Individual Process
- Active and Static Data
  - Real Time Data
  - Fixed Elements

Why make a digital twin?

- Reduce risk in experimentation
- Accelerate algorithm development
  - Research and Development
- Student use
  - Gathering data from the DT rather than the physical car

Methods/Results

Working Model

The current model represents an array of crucial automotive functions such as, forward, neutral, reverse, braking, accelerating (how much torque is being sent to the wheels), and cruise control. It is modeled to resemble the user dashboard found in the P1 car between the driver and passenger seats. In order to reach this stage, the process of building the model followed specific steps: skill acquisition, skill development, model development, and testing for efficacy. Understanding the functionality of the car along with becoming familiar with Simulink's programming language and Arduino allowed for the proper replication of the drivetrain of the P1 vehicle.

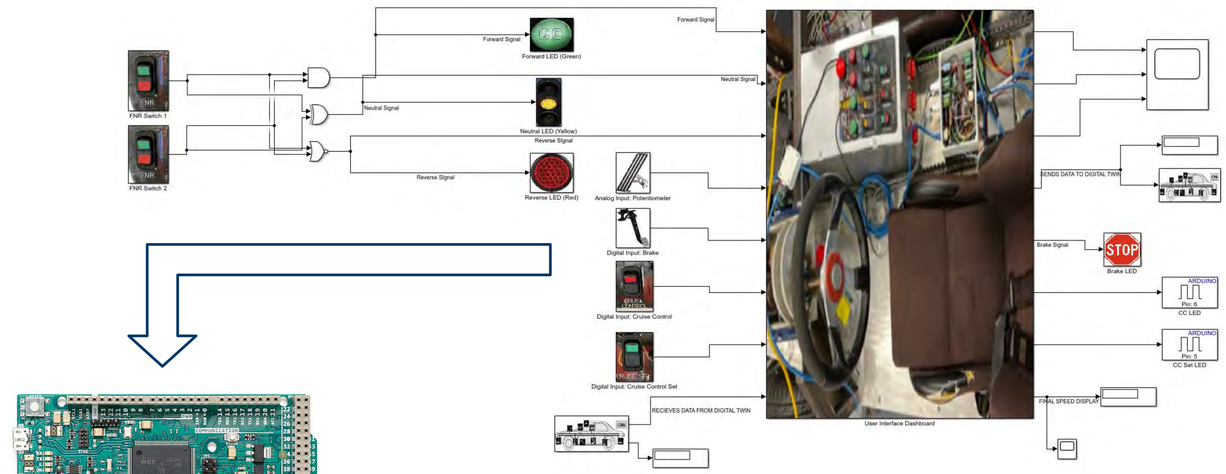

Digital Twin Side

The picture below illustrates the mathematical functions required to convert the torque being sent from the motor to the wheels into speed. Although not pictured here, the digital twin subsystem also calculates the maximum power produced at each speed as well as braking. This system depends on serial communication, a simple form of telecommunication that sends information bit by bit, to send signals from the user dashboard to the digital twin to perform the needed calculations to obtain the speed of the "car".

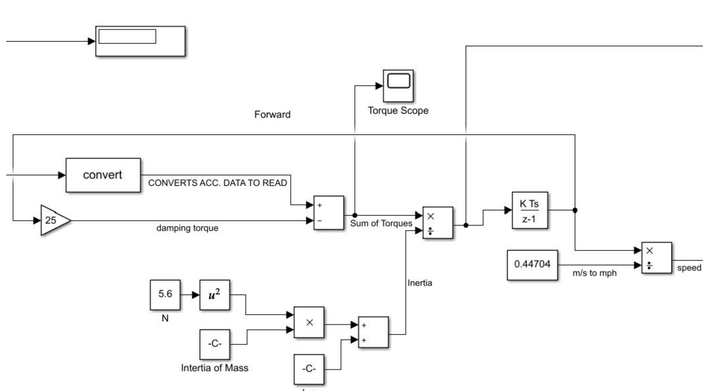

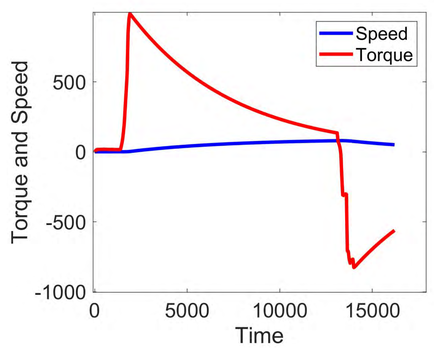

Digital Twin Experimental Data

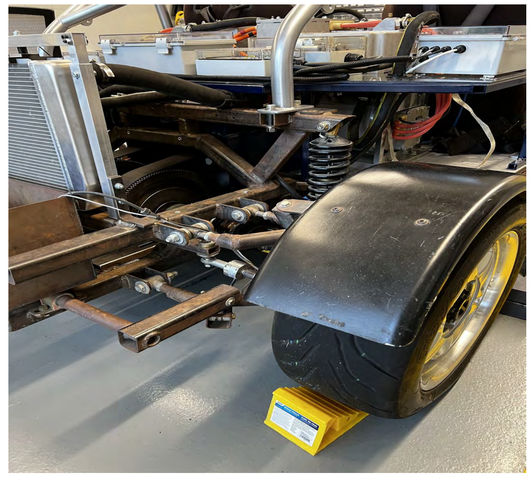

Drivetrain of the P1 Vehicle

Discussion

Outcome

- Working digital twin of the P1 Drivetrain
- Greatly improved proficiency in programming with Simulink and using Arduinos as an interface
- Gaining basic circuitry and electronics knowledge

Reflection

- Steep learning curves
- Considering pursuing a career in the automotive industry
  - Found personal enjoyment in the mechanical and digital aspects of working with a car
- Hope to use the problem solving skills learned during research and apply them in more areas

Future Recommendations

- Continue to expand the model
  - Complex features
  - Becoming more familiar with vehicle dynamics
  - Accounting for reactionary forces
- Compile findings for a conference paper
- Apply new knowledge to future Bucknell courses
- Obtain experimental data for testing

Acknowledgements

Research Mentor: Professor Craig Beal
Emerging Scholar Advisor: Dr. Margaret Marr

Assembly of Muon-Specific Particle Detectors

Cory Mabry & Dr Adam Hansell
Susquehanna University

Introduction

Cosmic rays are any collection of particles that penetrate our atmosphere from space. These streams of particles emit from celestial bodies at relativistic speeds meaning they carry enough energy to initiate high-energy collisions. These collisions with a molecule in our upper atmosphere will kickstart a reaction that yields a subatomic particle called a meson. Most commonly, the mesons that are yielded here will be the π (pion) or the K (kaon). Pions and kaons are unstable particles with very short lifetimes, meaning they will decay quite quickly. When one of these mesons decays, it can yield a muon. The muon itself is an elementary particle in the lepton family, meaning it does not seem to be composed of any other things. The muon is a sister particle to the more commonly known electron, both being leptons, and carries the same charge while flaunting about 200x greater mass. This greater mass gives it a stronger penetration power which allows it to be detected a bit more exclusively without interference of other subatomic particles. There is a rather constant flux of muons that came from this very series of events (shown in figure 2) all over Earth right now.

Goal

Our goal is to follow the pursuit of the CosmicWatch Project and build ourself a small and efficient muon detector for use at Susquehanna University. This is only step one, as we would like to use this first detector to test rates in different conditions and using different scintillators or overheads, etc. Once we've figured out which detector layout we wish to go further with, we hope to assemble an array of these in a 10x10 grid to track direction and zenith angle of particles detected!

Method

A block of plastic scintillator will be attached to a silicon photomultiplier to amplify the photon signal given off when a charged particle passes through a scintillator. This signal will be transmitted to our PCB via plugin connection and directed through a series of components into an Arduino Nano. The Arduino has been coded to interpret this signal and turn it into something readable for us. When the detector has detected any kind of signal, an LED will flash and time of incident will be marked which we can then look at through an SD card.

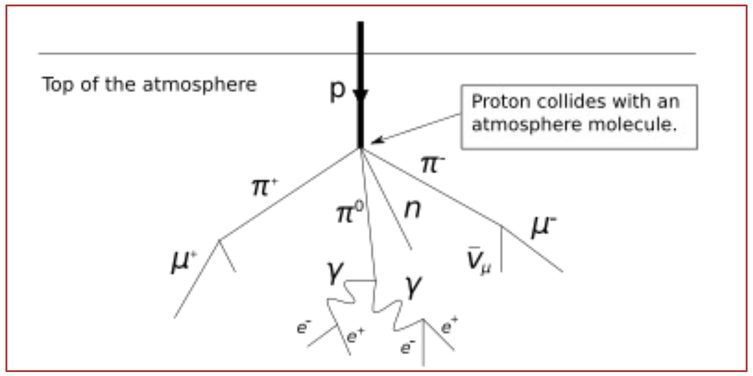

Figure 1 (above)

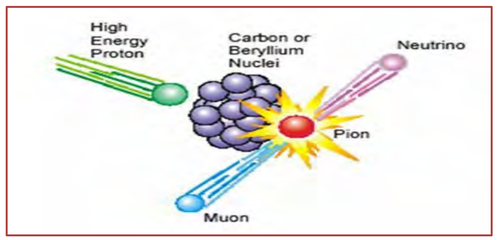

Figure 2 (below)

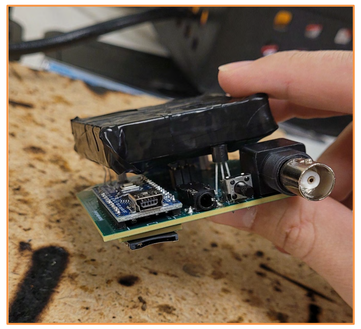

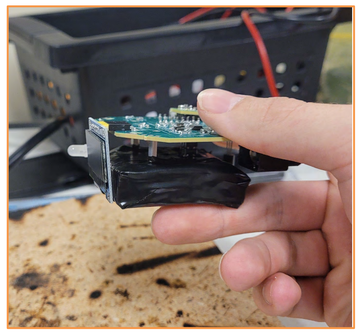

Figure 3

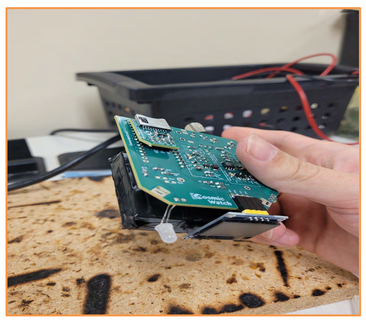

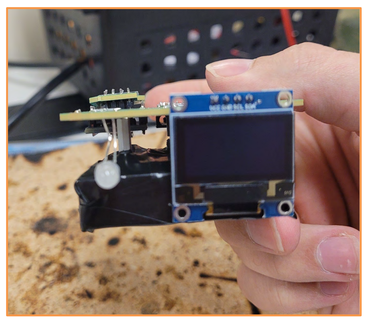

Shown in the image beside, the scintillator is wrapped in aluminum foil to ensure reflection of light and non-penetrative particles

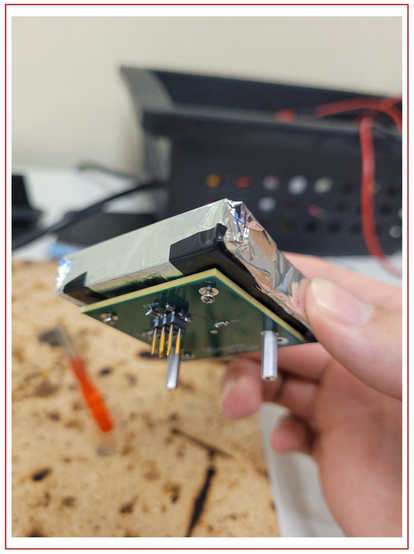

Progress/Conclusion

After the final steps of screwing the scintillator and SiPM together, light sealing the scintillator, and attaching the SiPM PCB to the main PCB via socket connection, a finished product was created (shown in fig. 3). The Arduino was attached to a power source and the code was uploaded but no results were being seen. This began the expected troubleshooting phase. Through a series of testing, the spot of error was narrowed down to a piece of the circuitry between the 6-pin receiver and the Arduino Nano. This, however narrowed it down far less than we hoped because this is exactly where the bulk of the components are. It's very possible I find the faulty piece before the summer ends, but if not, next summer will be the summer for finishing troubleshooting and collecting data.

Citation

Axani, Spencer Nicholas Gaelan. *The Physics behind the CosmicWatch Desktop Muon Detectors*. 2019.

Susquehanna UNIVERSITY

Medical Presentations of *GRIN2B*-Related Disorders

Dmitri Yarczower[1,2], Rebecca Smith, MS, CGC[1] & Cora M. Taylor, PhD[1]

[1]Geisinger, Autism & Developmental Medicine Institute, Lewisburg, PA
[2]Dickinson College, Carlisle, PA

Background

GRIN2B codes for the GluN2B protein and is essential for neuronal progenitor cell differentiation and is active in embryonic development.[3] When GluN2B is inhibited, neurons have an increased rate of dendrite pruning.[4]

GRIN2B developmental disorders are autosomal dominant and extremely rare. Penetrance estimate of pathogenic variants is 100%.[1] Most of the reported mutations are loss-of-function.[2] Emerging evidence suggests some variants cause a gain-of-function effect.

Methods

Simons Searchlight

- Online research study examining >170 genes that cause rare developmental conditions
- Receives and categorizes genetic information
- Connects genetic counselors with families to review medical and developmental history.
- Data is collected longitudinally.

Current Investigation

- Releasable data for participants with *GRIN2B* variants queried
- Data analyzed with basic quantitative statistics

Participants

57 Participants – Completed core medical history
47 Participants – Completed comprehensive medical history interview
19 months – 22 years of age

51 Sequence level variants
5 Partial deletions, 1 duplication
29 Pathogenic, 28 Likely Pathogenic

Results

- All participants presented with an intellectual disability with some degree of variation in its severity.
- The most common condition categories seen are intellectual disability, neurological, gastrological, and visual.

- GERD and strabismus occurs in 51% of participants.
- Otitis media and constipation occur in 57% of participants.
- 91% of participants reported hypotonia.

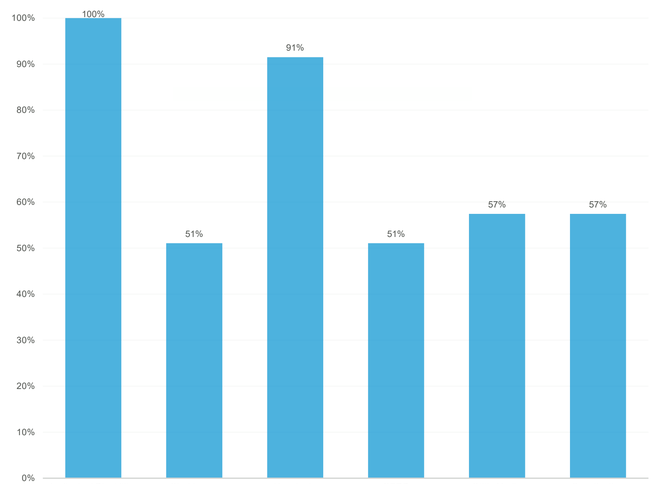

Figure 2: Comprehensive Medical History Interview (N=47)

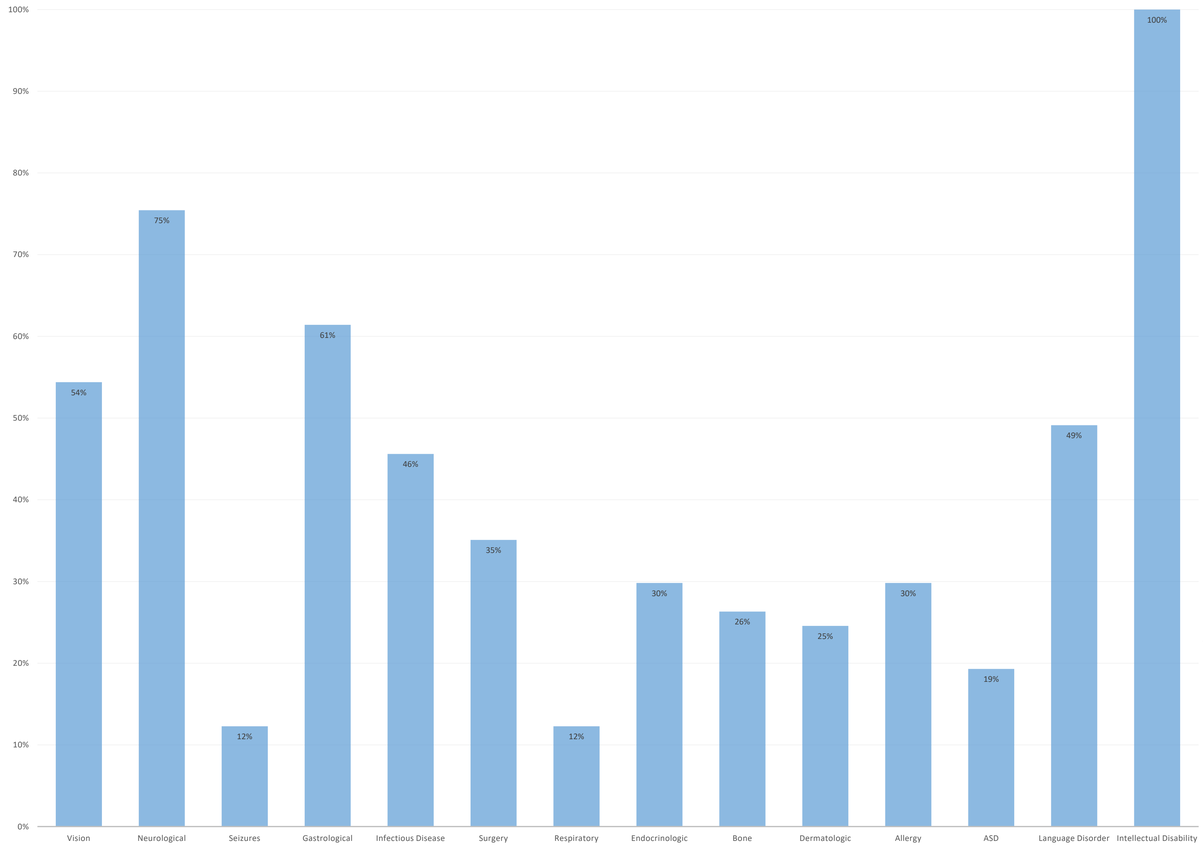

Figure 1: Core Medical History (N=57)

Discussion

This work builds on existing literature showing most common features of GRIN2B related disorder. Intellectual disability, hypotonia, and epilepsy have already been associated with *GRIN2B* mutations.[2]

Building on the information known in the literature, this data demonstrates additional systemic features of *GRIN2B*-related disorder. Among body systems, participants report neurological, gastrointestinal, and visual features. Upon more detailed assessment, specific features include: hypotonia, otitis media, constipation, GERD, and strabismus.

Conclusion

This work helps to elucidate additional areas of medical care relevant to patients with *GRIN2B*-related disorder.

All variants were classified as disease causing but, in some cases, we did not know the mechanism (loss or gain) of the variant. There is limited information on adults, most of the data is related to pediatrics; we don't know the long-term course of the disorder.

Future research should focus on evaluating differences between loss and gain of function and better understanding variability in presentation. *GRIN2B* mutations could be studied for their mechanisms of action in potentially contributing to these conditions.[5]

References

1. Platzer K, Lemke JR. GRIN2B-Related Neurodevelopmental Disorder. 2018 May 31 [Updated 2021 Mar 25]. In: Adam MP, Mirzaa GM, Pagon RA, et al., editors. GeneReviews® [Internet]. Seattle (WA): University of Washington, Seattle; 1993-2022. Available from: https://www.ncbi.nlm.nih.gov/books/NBK501979/
2. Chun Hu, Wenjuan Chen, Scott J. Myers, Hongjie Yuan, Stephen F. Traynelis, Human GRIN2B variants in neurodevelopmental disorders, Journal of Pharmacological Sciences, Volume 132, Issue 2, 2016, Pages 115-121, ISSN 1347-8613, https://doi.org/10.1016/j.jphs.2016.10.002. (https://www.sciencedirect.com/science/article/pii/S1347861316301335)
3. Bell, S., Maussion, G., Jefri, M., Peng, H., Theroux, J. F., Silveira, H., Soubannier, V., Wu, H., Hu, P., Galat, E., Torres-Platas, S. G., Boudreau-Pinsonneault, C., O'Leary, L. A., Galat, V., Turecki, G., Durcan, T. M., Fon, E. A., Mechawar, N., & Ernst, C. (2018). Disruption of GRIN2B Impairs Differentiation in Human Neurons. *Stem cell reports*, *11*(1), 183–196. https://doi.org/10.1016/j.stemcr.2018.05.018
4. Bahry Jacob A., Fedder-Semmes Karlie N., Sceniak Michael P., Sabo Shasta L, An Autism-Associated de novo Mutation in GluN2B Destabilizes Growing Dendrites by Promoting Retraction and Pruning, Frontiers in Cellular Neuroscience, Volume 15, 2021, https://www.frontiersin.org/article/10.3389/fncel.2021.692232, DOI: 10.3389/fncel.2021.692232, ISSN 1662-5102.
5. Bernier, R., Golzio, C., Xiong, B., Stessman, H., Coe, B., Penn, O., Witherspoon, K., Gerdts, J., Baker, C., Vulto-van Silfhout, A., Schuurs-Hoeijmakers, J., Fichera, M., Bosco, P., Buono, S., Alberti, A., Failla, P., Peeters, H., Steyaert, J., Vissers, L., . . . Eichler, E. (2014). Disruptive CHD8 Mutations Define a Subtype of Autism Early in Development. *Cell*, *158*(2), 263–276. https://doi.org/10.1016/j.cell.2014.06.017

Turbidity Estimation Based on Sampled Images of Reference and Test Water Samples

Bucknell UNIVERSITY

Ding Zhang, Prof. Alan Marchiori

Department of Computer Science, Bucknell University, Lewisburg, PA.

Introduction

Water quality monitoring is the process by which critical characteristics of water (physical, chemical, biological) are measured. One of the universal metrics and notable indications of water quality is **turbidity**. The standard unit widely used for turbidity measurement is called the nephelometric turbidity unit (NTU). The current measurement of turbidity often involves the use of a turbidimeter, including Hach 2100Q. They are highly accurate with a wide range of NTU and high resolution, however, these types of equipment are often used for laboratory water quality analysis and would cost thousands of dollars.

Research Objective:

We aim to develop a low-cost water turbidity estimation system by analyzing sampled images using image processing techniques.

Theory & Tools

- ***Theory***:
  - When light passes through suspended particles in water, attenuation and scattering will occur at all directions, which includes direct beam ($\boldsymbol{\theta}$ = 0°), forward scattering ($\boldsymbol{\theta}$ < 90°), side scattering ($\boldsymbol{\theta}$ = 90°), and back scattering (90° < $\boldsymbol{\theta}$ < 180°) [2].
  - In particular, we focus on **side scattering**, where we place our camera perpendicular to the LED light beam (fig 1), facing the water samples.
- ***Tools:***
  - Our holder is 3D-printed with two openings for holding the water samples: reference and test samples. It is attached to an electronic board that has two LEDs (fig 2).

Figure 1. Sampled Image

Figure 2. 3D-printed container for holding water samples

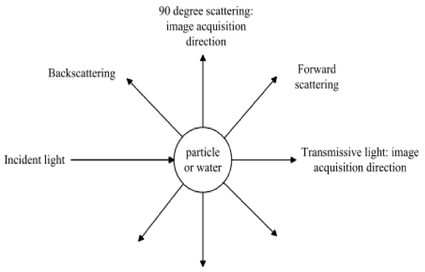

Figure 3. The principle of light attenuation in turbid water

Hypothesis

One novel approach of our research is that we calculated **the difference between the reference and the test sampled images' mean pixel intensity** to achieve turbidity estimation.

- We purpose that within the region of interest (ROI), the pixel intensity tend to present an effect of gradient descent, from bottom pixels to top, since attenuation occurs more frequently when closer to the LED.
- Then the difference between the arithmetic mean of the reference and the test sample pixel intensity would become a meaningful parameter to fit into the model.

$$\overline{diff} = \frac{\sum_{bottom}^{top}\sum_{left}^{right} greyscale((test-ref))}{(top-bottom)\times(right-left)}$$

- We assume that by having a reference sample, the result would be **less subjective to environmental factors** (angle, position, and lighting).

General Methodology

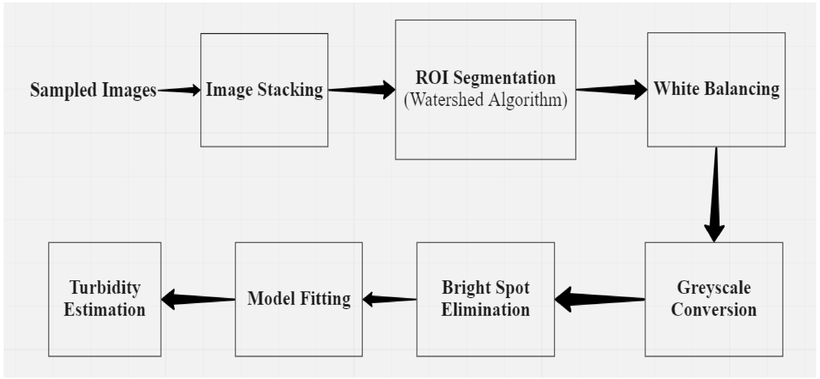

Experimental Results

- Approximately linear relationship between turbidity and mean pixel intensity:

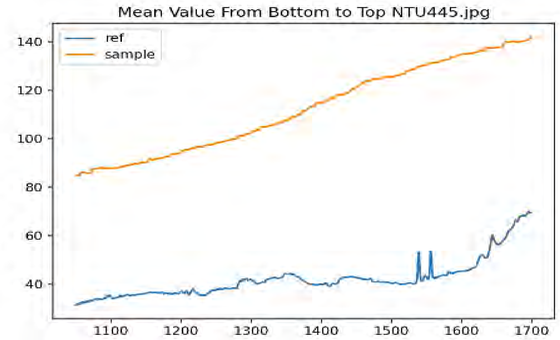

- Our model exhibits a linear relationship between pixel intensity (x-axis) and the turbidity (NTU):

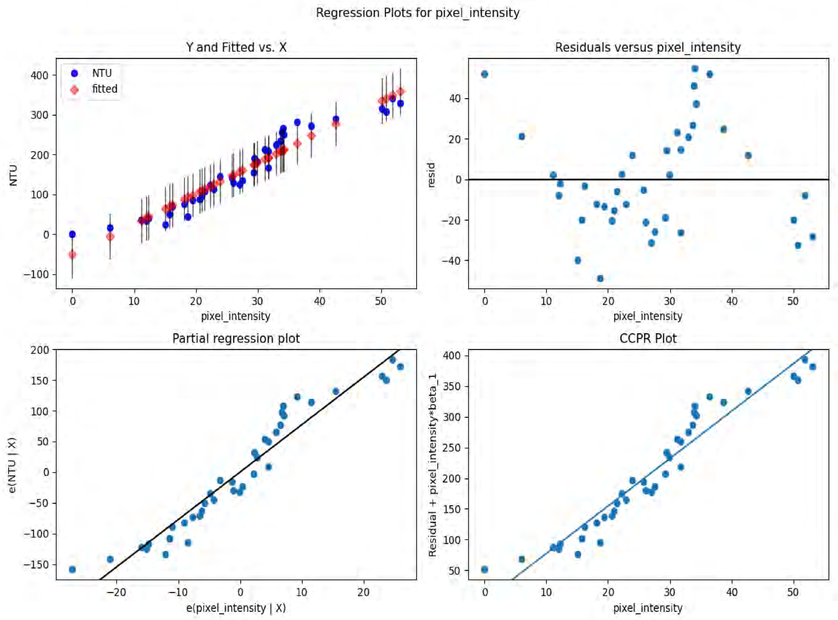

Conclusion

- We have proved our hypothesis that the sampled images present gradient descent with a linear relationship, and our model also shows **a very standard linear relationship** between **mean pixel intensity and the turbidity (NTU).**
- By fitting linear regression, our model has reached an R^2 value of 0.986.

OLS Regression Results

Dep. Variable:	Estimated	R-squared:	0.987
Model:	OLS	Adj. R-squared:	0.986
Method:	Least Squares	F-statistic:	1454.
Date:	Sun, 17 Jul 2022	Prob (F-statistic):	2.04e-19
Time:	15:00:42	Log-Likelihood:	-83.878
No. Observations:	21	AIC:	171.8
Df Residuals:	19	BIC:	173.8
Df Model:	1		
Covariance Type:	nonrobust		

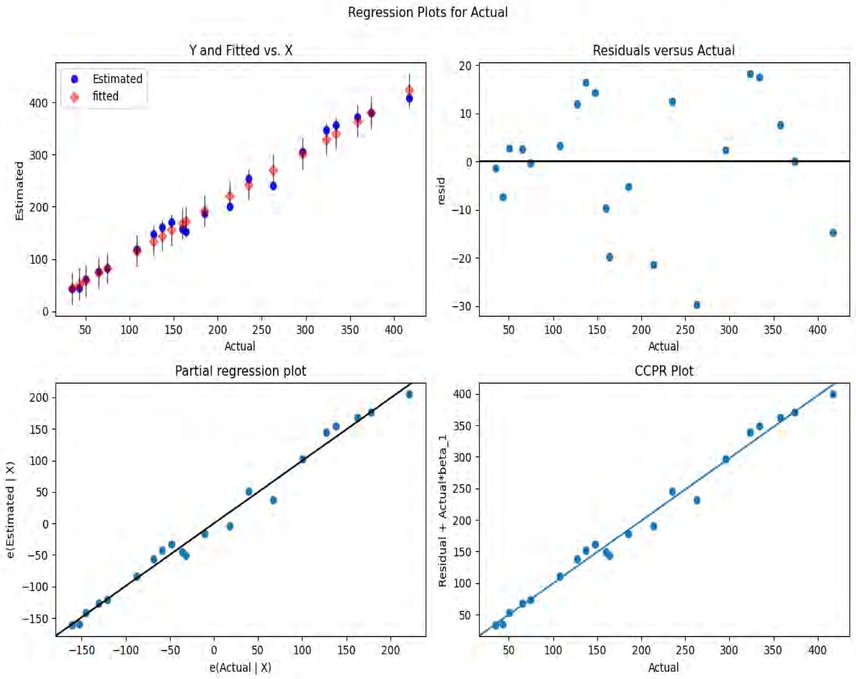

- In actual experiment, our approach of having a reference sample was indeed less subject to certain environmental factors, such as filming angle and sample position, but lighting condition would still impact the estimation output, causing an error of at most 50 NTU. Despite this, compared with having only a test sample, our two samples did contribute significantly to the accuracy of our final result.

References

1. "WHO-FWC-WSH-17.01-Eng.Pdf," accessed July 5, 2022, https://apps.who.int/iris/bitstream/handle/10665/254631/WHO-FWC-WSH-17.01-eng.pdf?sequence=1&isAllowed=y.
2. Yeqi Liu, Yingyi Chen, and Xiaomin Fang, "A Review of Turbidity Detection Based on Computer Vision," IEEE Access 6 (2018): 60586–604, https://doi.org/10.1109/ACCESS.2018.2875071.

Characterizing Familial Hypercholesteremia in the NIH AllofUS Cohort

Nuha Mohammed, Alexander Berry, PhD, Matthew Oetjens, PhD
Geisinger Medical Center, Danville, PA

Introduction

- Familial hypercholesterolemia (FH) is an inherited disorder characterized by lifelong elevated low density lipoprotein cholesterol (LDL-C) and dramatically increased risk for premature atherosclerotic cardiovascular disease (ASCVD).

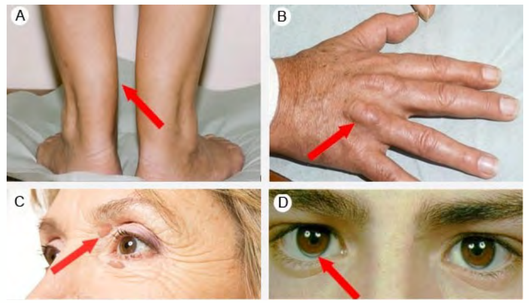

Figure 1 –Patients with untreated FH may experience Xanthomas on the Achilles *tendons (A), metacarpal phalangeal extensor tendons of the hands (B), and corneal arcus, a white or gray ring around the iris of the eye (C & D). Image retrieved from* https://www.athero.org.au/fh/health-professionals/how-to-diagnose-fh/.

- Genetic studies now suggest that FH encompasses five discrete subtypes based on LDL-c levels and 1) a monogenic FH variant, 2) a high low density lipoprotein cholesterol (LDL-c) polygenic score, 3) elevated lipoprotein(a), 4) elevated LDL-c polygenic score with elevated lipoprotein(a), and 5) a positive family history without an identifiable genetic cause, or true "phenotypic FH."
- The primary question of this project is: Are there differences in treatment, comorbidities, and ASCVD outcomes between FH subtypes?
- We explore the prevalence of FH in the NIH AllofUs cohort to scope the utility of the AllofUs cohort for studying FH

Geisinger

What is AllofUS?

- NIH-funded research program gathering health data from millions of people in the U.S.
- Designed to support and accelerate health care research by providing qualitative and quantitative data pertaining to lab measurements, genome sequencing, and drug exposure, among many others, pulled from electronic health records and testing.

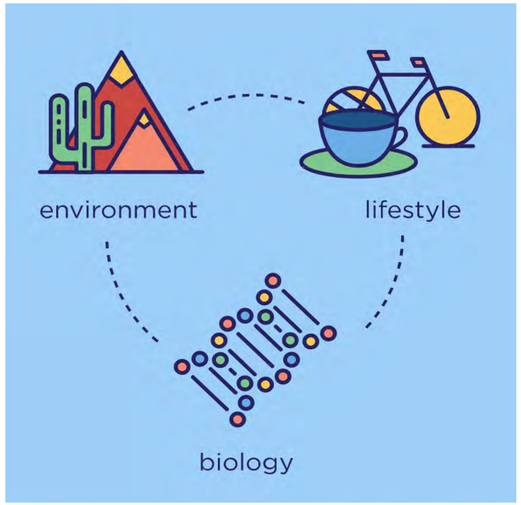

Figure 2 – AllofUS aims to bring together data allowing for analysis of the interplay between effects of environment, lifestyle and biology on health. Image retrieved from https://allofus.nih.gov/.

Materials and Methods

1. Restricted samples to those containing whole-genome sequence data
2. Defined familial hypercholesterolemia with a threshold of: LDL-C>=190 indicating FH.
3. If exposed to statins, we adjusted the LDL-C by dividing by 0.7 to reflect pre-statin exposed values.

Materials and Methods

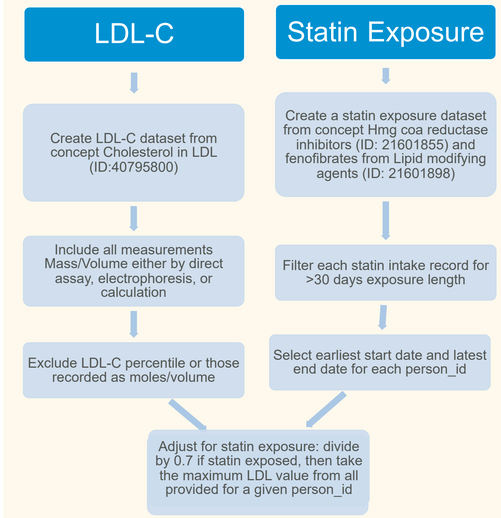

Figure 3 – LDL-C and Statin Exposure data were pulled from the AllofUS cohort using the concept identifiers, as described. Statin exposure was defined specifically, and LDL values were adjusted if statin exposure was determined by our criteria.

Results and Discussion

- We analyzed the 506,260 participants in the AllofUs cohort. Of these, 21.05% had a recorded LDL-C value
- Next, we measured the prevalence of the FH phenotype by identifying the number of individuals with an LDL-C >=190 mg/dL.
- We found that 19.25% of individuals with LDL-measurements had at least 1 LDL-C consistent with the FH phenotype.
- Lastly, to determine the relationship between FH and statin treatment, we compared adjusted LDL-C values in statin exposed to statin unexposed.

Results and Discussion

- On average, adjusted statin-treated values were (24 mg/dL) higher than untreated, consistent with their use for hypercholesteremia.

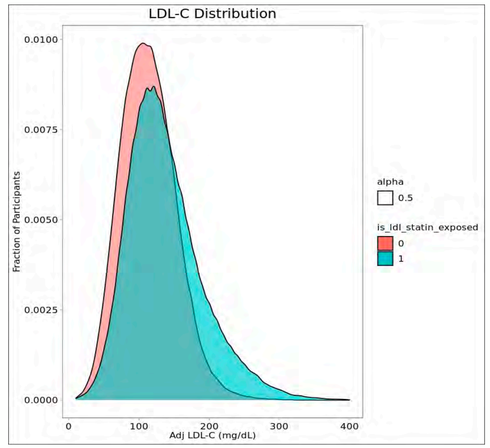

Figure 4 – Distribution of low-density lipoprotein cholesterol between statin-exposed and statin-unexposed groups within the selected cohort participants.

Future Direction

- Screen all individuals with whole genome sequences available for monogenic variants
- Stratify data by FH-subtype using labs, drug exposure, and whole genome data
- Determine comorbidities and ASCVD outcomes using EHR Data
- Perform regression analyses to compare ASCVD risk between FH-subtypes

References

1. A. H. Ramirez, K. A. Gebo, P. A. Harris, Progress With the All of Us Research Program: Opening Access for Researchers. *JAMA***325**, 2441–2442 (2021).
2. A. J. Berberich, R. A. Hegele, The complex molecular genetics of familial hypercholesterolaemia. *Nat. Rev. Cardiol.* (2018) https://doi.org/10.1038/s41569-018-0052-6.
3. D. J. Carey, *et al.*, The Geisinger MyCode community health initiative: an electronic health record-linked biobank for precision medicine research. *Genet. Med.***18**, 906–913 (2016).

The Effect of Acute Stress on Context-Dependent Memory in Rats

Abigail R. Wagner & James F. Briggs

Susquehanna University

Introduction

- Stress has been shown to both enhance and impair learning.
- Stress has also been shown to impair the retrieval of extinction learning.
  - Extinction is when a learned behavior is gradually weakened, and eventually stops, due to the lack of a reinforcer.

Why does stress impair extinction?

- One hypothesis is that stress impacts the ability to process context (the environment where learning takes place).
  - Extinction has been found to be context-specific, meaning that the behavior may return when in an environment separate from where extinction took place.
- Given this information, we sought to evaluate whether acute stress has an impact on the context-shift effect.
  - The term "context-shift effect" is used to explain the decrement in performance observed when there is a difference between where learning and testing take place.

Method

- *Subjects.* Forty male, Long-Evans rats were used as subjects.
- *Apparatus & Context.* Training and testing were conducted in a shuttle box, divided into two compartments by a sliding door (shown below). Two boxes were used, each one placed in a different room with distinct environments (Context A or Context B).

Figure 1. Image of a shuttle box typically used in passive avoidance testing.

- *Procedure.*
  - Stress – Two of the four groups received one hour of restraint stress 48-hours prior to training (See Table 1).
  - Training – All groups were trained in either Context A or B. Each rat was placed in the white side of the shuttle box with the center door closed. The door then opened, allowing the rat to cross to the black side. Upon entering the black side, the door was closed and a single footshock was delivered. This induced fear to the black side.
  - Testing – All groups were tested for fear of black compartment 24 hours after training. Each rat was placed in the white side of the box. Once the center door opened, it remained open for 5 minutes. The amount of time taken for the rat to cross to the black compartment was recorded as the dependent measure.

Table 1. Experimental design for Experiment 1

Group	Stress	*48 hr*	Training	*24 hr*	Test
Same	No		Context A		Context A
Shift	No		Context A		Context B
Stress/Same	Yes		Context A		Context A
Stress/Shift	Yes		Context A		Context B

Note – Contexts A and B were counterbalanced for each group

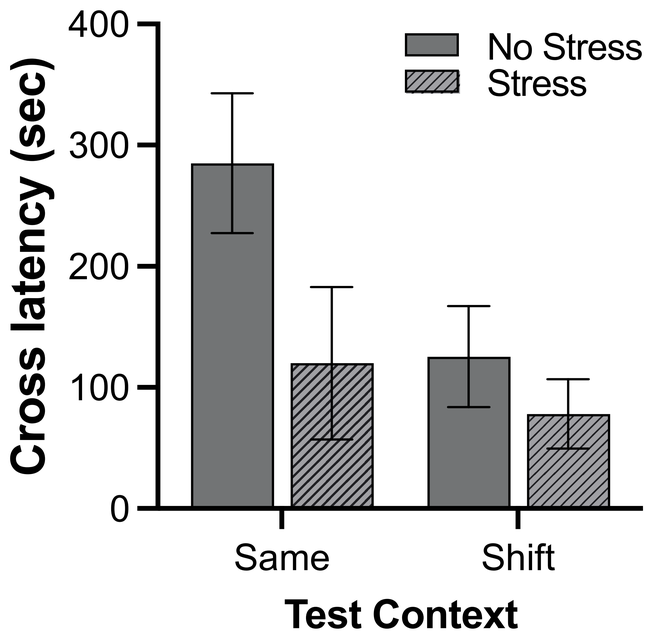

Figure 2. Average crossing latency (in seconds) of rats in a passive avoidance chamber.

Results

- A 2(no stress, stress) x 2(same, shift) ANOVA was calculated on test latencies.
- A significant main effect of stress was found [($F(1,36) = 4.591$, $p = .039$].
- A significant main effect of context was found [($F(1,36) = 4.121$, $p = .050$].
- The interaction between stress and context was not significant [($F(1,36) = 1.412$, $p = .243$].
- The same and shifted context rats from the no stress group differed in cross latency time [$t(18) = 2.241$, $p = .038$].
- The same and shifted rats from the stress group did not differ in cross latency time [$t(18) = .605$, $p = .553$].

Discussion and Conclusion

- Stressed rats that remained in the same context for testing and training had cross times similar to the unstressed rats that changed contexts.
- The significant main effect of stress shows that stress impacted the context shift.
- The significant main effect of context also demonstrates context-dependent retention.
  - Results show a context shift among non-stressed rats, but not for the stressed group.
  - This suggests that stressed rats were unable to process their environment during training and unable to recognize it during testing.
  - The testing context, even if the same, was treated as a new environment.
- This would explain why stressed rats exhibited quick cross times in both same and different environments.
- Possible limitations:
  - Only male rats were used – female rats have been found to generalize more.
  - A limited number of rats was used in the experiment.
  - This study does not determine how stress impacts extinction but gets us closer to understanding how.
  - Further research is needed.
    - Must be able to demonstrate these results in humans.
- It is important to understand how stress and extinction are affected by context, as they are used in exposure-based therapies to treat anxiety disorders.

Susquehanna UNIVERSITY

Get-2-Goal Diabetes App:
Estimating Risk and Remission

Kate Strong
Advisor: Prof. Lea Wittie

Bucknell UNIVERSITY
Computer Science Department
2022

BACKGROUND

- Obesity is considered a global epidemic, affecting more than 40% of US adults.
- Obesity is associated with increased risk for type 2 diabetes and other medical comorbidities.
- Bariatric surgery leads to substantial weight loss and often, to the remission of type 2 diabetes.

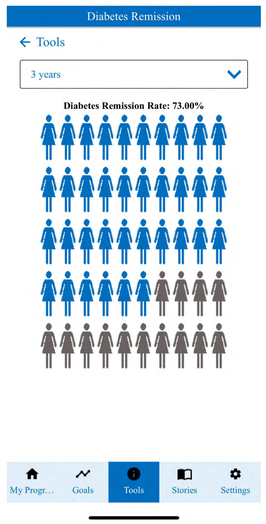

Figure 1. Screenshot showing 3-year diabetes remission among bariatric surgery patients based on patient demographics.

- Get-2-Goal app is joint collaboration between the Geisinger Obesity Institute and Bucknell CS Department.
- This app helps healthcare providers and patients in making decisions about whether to perform bariatric surgery
- The app also tracks the recovery process after surgery including remission of type 2 diabetes.

The existing Get-2-Goal app is undergoing revisions to refine the diabetes remission calculator and develop a new risk calculator.

APPROACH

- Learned languages: Javascript, HTML, CSS.
- Installed Cordova and android emulator.
- Reviewed existing code and mapped out existing functions.
- Presented at weekly interdisciplinary team meetings with Geisinger Obesity Institute and Bucknell CS Department.

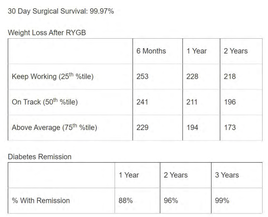

30 Day Surgical Survival: 99.97%

Weight Loss After RYGB

	6 Months	1 Year	2 Years
Keep Working (25th %tile)	253	228	218
On Track (50th %tile)	241	211	196
Above Average (75th %tile)	229	194	173

Diabetes Remission

	1 Year	2 Years	3 Years
% With Remission	88%	96%	99%

Figure 2, Screenshot showing survival, weight loss and diabetes remission from Get-2-Goal website.

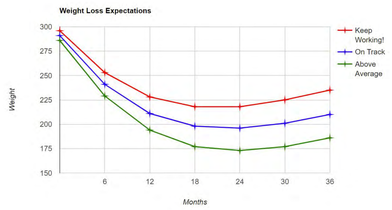

Figure 3. Screenshot showing weight loss trajectories.

RISK AND REMISSION CALCULATORS

- Was responsible for updating the existing diabetes remission calculator (DiaRem2, right) based on the published literature.

Scoring algorithm for DiaRem2

Step 1: Calculate DiaRem2 score. Collect patient age, A1c, T2DM medications, and reported duration of T2DM	Time with T2DM (years)		
	≤ 5	6 – 9	10+
Age (years)			
< 40	0	0	0
40 – 49	1	1	1
50 – 59	2	2	10
≥ 60	4	4	10
HbA1c (%)			
<6.5%	0	0	0
6.5 – 6.9%	2	5	5
7.0 – 8.9%	2	10	10
≥ 9.0%	10	10	10
Treatment with insulin			
No	0	0	0
Yes	5	5	5
DiaRem2 Score	Sum of above		

Step 2: Assign remission group	**DiaRem2 Remission group**
DiaRem2 score 0 – 5	High
DiaRem2 score 6 – 12	Intermediate
DiaRem2 score 13 – 25	Low

T2DM=Type 2 diabetes; A1c=Hemoglobin A1

- Also responsible for implementing a separate diabetes risk calculator (DiaGet, below) as a new website to complement the app.

$$\frac{Prob(progression\ to\ diabetes)}{1 + exp\,(-31.367 + 0.0369 * BMI - 0.00044 * Age + 0.372 * Male + 4.741 * A1c - 0.0755 * PercWL + 0.6419 * Gest\ DM)} = \frac{exp\,(-31.367 + 0.0369 * BMI - 0.00044 * Age + 0.372 * Male + 4.741 * A1c - 0.0755 * PercWL + 0.6419 * Gest\ DM)}{1 + exp\,(-31.367 + 0.0369 * BMI - 0.00044 * Age + 0.372 * Male + 4.741 * A1c - 0.0755 * PercWL + 0.6419 * Gest\ DM)}$$

SUMMARY OF PROGRESS

- Implemented DiaRem2 for app and web browser.
- Developed tests for DiaRem2 for app and web browser using all possible patient profiles.
- New diabetes risk calculator website under development.
  - target completion: August 2022

FUTURE CONSIDERATIONS

- Moving forward, we will continue to work on the risk calculator website.
- Bug fixes will also be a priority.
- As we refine the interface, we may solicit input from patients, providers, and other key stakeholders.
- It will also be important to collect data on patient choices and outcomes.

ACKNOWLEDGEMENT

Thanks to the Joseph A. Ciffolillo ’61 Healthcare Technology Inventors Program (HTIP)

REFERENCES

1. CDC (2021). National Health and Nutrition Examination Survey 2017–March 2020 Prepandemic Data Files Development of Files and Prevalence Estimates for Selected Health Outcomes, National Health Statistics Reports.
2. 2. Bailey-Davis L, Wood GC, Cook A, Cunningham K, Jamieson S, Mowery J, Naylor A, Rolston DD, Seiler C, Still CD. Communicating personalized risk of diabetes and offering weight reduction program choice: Recruitment, participation, and outcomes. Patient Educ Couns. 2021 May;104(5):1193-1199.

Usability of the Get-2-Goal App

Julia Calderone

Bucknell University
Computer Science Department
2022

INTRODUCTION

- The Get-2-Goal project is a collaboration between Bucknell undergraduate students, Bucknell's CS Department, and Geisinger's Obesity Center
- The app provides tools for Geisinger patients seeking to track their weight loss and health details, both before and after Bypass or Sleeve surgery
- Major functions of the app include an individualized goals graph, survival rate calculator, diabetes remission calculator, and weight log
- **Usability**: an assessment of how effective and understandable user interfaces are to use
  - Usability is a common factor when it comes to interacting with apps

Figure 1. An individualized goals graph, tracking weight loss after surgery.

Figure 2. A comparison graph, which compares the outcomes of Bypass vs. Sleeve surgery.

My task focuses on gauging how well individuals can interpret the graphs and functions within the Get-2-Goal app. If the data that we are presenting is not understandable or readable, the app will not be effective for its users. After continuously analyzing the app and conducting a survey, I can revise the existing Get-2-Goal app to include more usable features and present our data in a more understandable manner.

DATA COLLECTION: SURVEY

- In order to create and conduct this survey, I completed CITI Ethics training for IRB certification
- I created a survey that asked participants to interpret the graphs and visuals displayed in the Get-2-Goal App
  - If participants could not understand them, we would clearly need to make a change in the way we present data to our users
- The survey was in the form of a Google Form and multiple choice format
- Each question referred to a visual from the app and asked the participant to pick the interpretation that best match their own
- Participants are Bucknell students

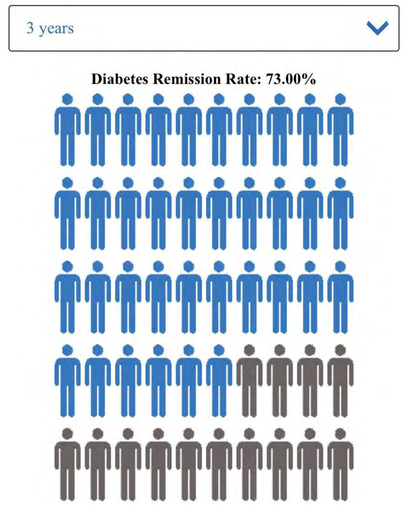

Figure 3. A diabetes remission chart which conveys this individual has a 73% chance of going into remission after weight loss surgery.

Figure 4. An individualized goals table, which tracks your weight loss progress after surgery.

SURVEY RESULTS

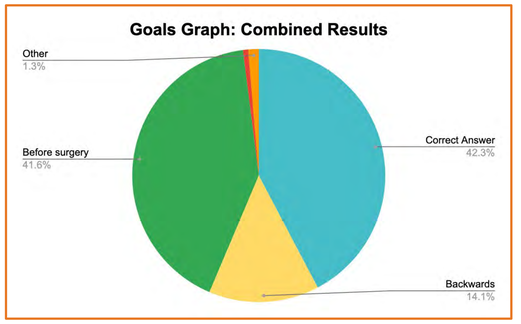

Figure 5. A chart that shows how well participants interpreted each question about the goals graph.

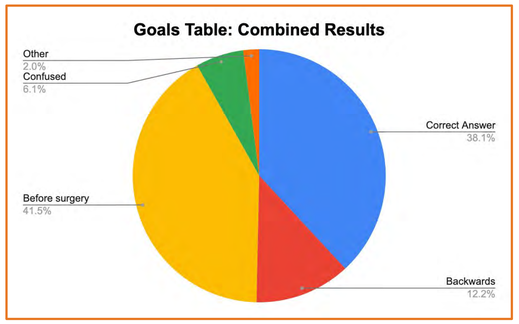

Figure 6. A chart that shows how well participants interpreted each question about the goals table.

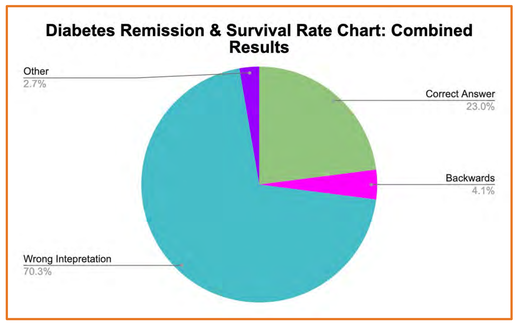

Figure 7. A chart that shows how well participants interpreted the questions about the diabetes remission and survival rate charts.

FUTURE CONSIDERATIONS

- I plan to make a number of updates to the app to improve usability, including:
  - Updating and clarifying graph title
  - Adding an information button users can click to get more information on graphs
  - Replacing the data table
  - Adding labels to graphs & visuals

REFERENCES

1. https://www.citiprogram.org/members/index.cfm?pageID=50

Comparison of Orientation-Specific and Traditional Measures of Subthalamic Nucleus Activation

Matthew Kroen, Karlo A. Malaga, Ph.D.

Department of Biomedical Engineering, Bucknell University, Lewisburg, PA

Introduction

- Parkinson disease (PD) is a degenerative disease that is characterized by a gradual loss of motor control.
- Deep brain stimulation (DBS) of the Subthalamic Nucleus (STN) is one option for treating the disease and involves surgically inserting a lead into the brain near the STN in order to electrically stimulate the STN.
- Volume of tissue activation (VTA) modeling is used to determine what portions of the brain are being stimulated.
- DBS of the STN is typically targeted towards the dorsolateral STN, the approximate location of the sensorimotor STN [2] (Figure 1). However, how to define what the targeting location is still under debate [1].

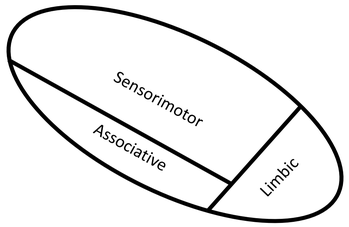

Figure 1: Approximate STN functional zones from a coronal view.

Objective

To determine if defining stimulation location based on the overall orientation of the STN provides a better correlation towards clinical outcome than the traditional method does.

Methods

- 40 PD patients underwent bilateral STN-DBS with their STN boundaries being preoperatively recorded.
- VTAs were calculated using recorded tissue conductivities, electrode contact locations, and stimulation settings [3] for 72 of the 80 total hemispheres (Figure 2).
- Each STN was segmented into the six anatomical directions based on a voxel's location relative to the STN centroid and enclosed within a Minimum Volume Enclosing Ellipsoid to produce orientation-specific anatomical directions (Figure 3).
- Segment activation was calculated using the overlap of the VTA and STN.

$$\text{Segment activation (\%)} = \frac{Number\ of\ segment\ points\ inside\ the\ VTA}{Total\ number\ of\ STN\ points} x\ 100$$

- For each patient, the treatment's resulting motor improvement as measured by the Unified Parkinson's Disease Rating Scale (UPDRS) was used to calculate the overall percent improvement for the treatment.
- Segment percent activation and percent improvement were compared to determine if the orientation-specific approach demonstrated better correlations.

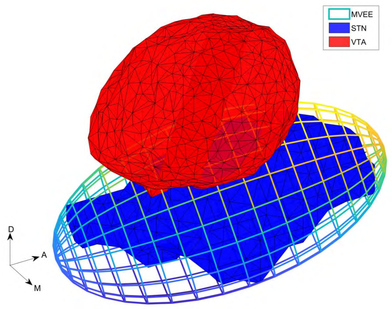

Figure 2: Patient's STN, enclosed by the corresponding MVEE, along with the VTA produced by the patient's DBS treatment

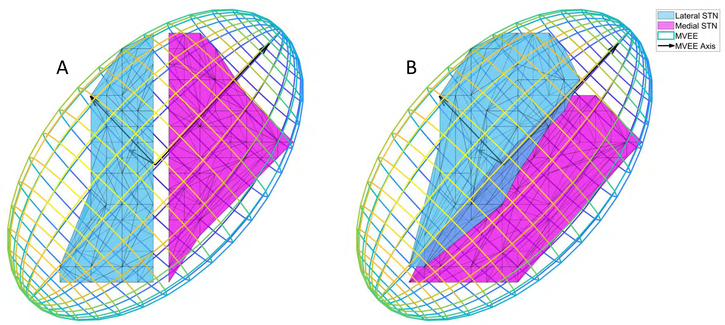

Figure 3: Lateral and Medial STNs as defined via the traditional centroid method (A) and an orientation-specific method based on a Minimum volume enclosing ellipsoid (B).

Results

- Ventral (p = 0.001) and Anterior (p = 0.03) directions demonstrated significant differences in percent activation between the traditional and orientation specific methods.
- Motor improvement and STN activation correlations were decreased for the orientation-specific method versus the traditional method in the ventral and anterior directions (Figure 4).
- In the ventroanterior direction, the orientation-specific method demonstrated an improved correlation versus the traditional segmentation, but the correlation was not significant (Figure 4).

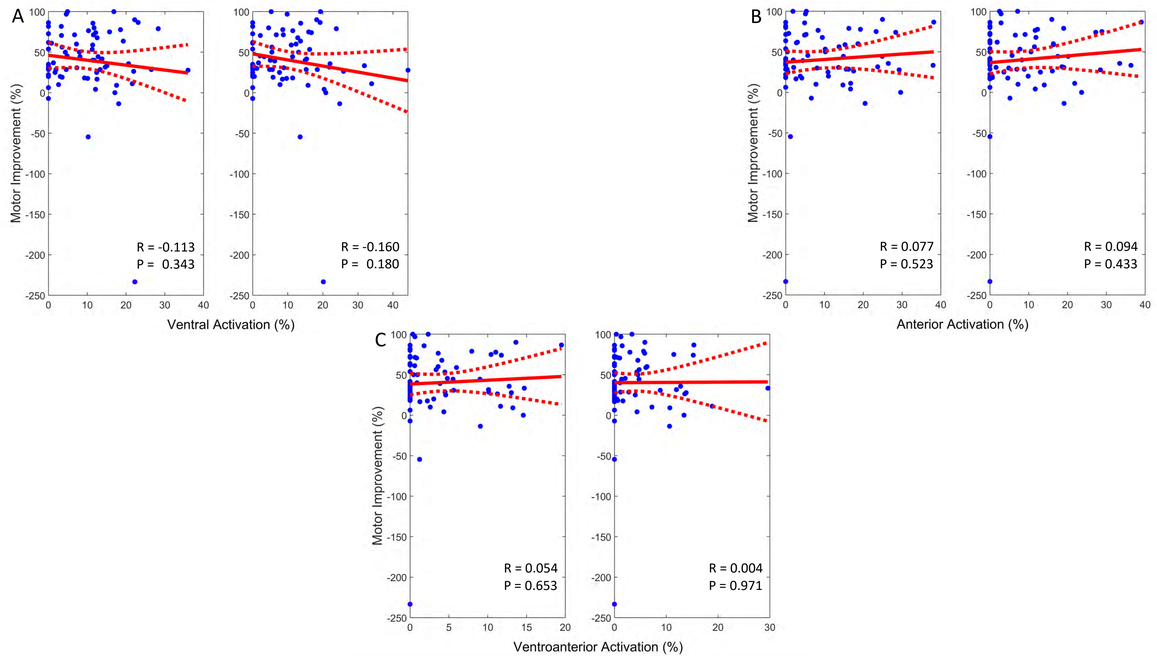

Figure 4: Linear regressions comparing the traditional method of defining directions (Right) and the orientation-specific method (Left) to overall motor improvement when looking at the ventral (A), anterior (B), and ventroanterior (C) segments of the STN.

Discussion

- This orientation-specific method appears comparable, but not superior to the traditional method.
  - Increased effort to segment the STN based on the orientation for little benefit presents few use cases for this approach.
- This method focused on the overall STN structure, a method that more closely follows the functional zones (Figure 1) may prove superior.

References

1. Coenen, V. A., Prescher, A., Schmidt, T., Picozzi, P., & Gielen, F. L. H. (2008). What is dorso-lateral in the subthalamic Nucleus (STN)? - A topographic and anatomical consideration on the ambiguous description of today's primary target for deep brain stimulation (DBS) surgery. *Acta Neurochirurgica*, *150*(11).
2. Eduardo E. Benarroch (2008). Subthalamic nucleus and its connections, anatomic substrate for the network effects of deep brain stimulation. *Neurology*, *70*(21).
3. Malaga, K. A., Costello, J. T., Chou, K. L., & Patil, P. G. (2021). Atlas-independent, N-of-1 tissue activation modeling to map optimal region of subthalamic deep brain stimulation for Parkinson disease. *NeuroImage. Clinical*, *29*.

Acknowledgements

The authors would like to thank the patients involved in this study for their voluntary participation, and Parag G. Patil, M.D., Ph.D., Kelvin L. Chou, M.D., Aidan Ahamparam, and Joseph T. Costello from the University of Michigan for the clinical data used in this project. Funding for this research was provided by the Bucknell University's Emerging Scholars Summer Research, Scholarship, & Creativity program.

Contact Information

Computational Neuromodulation Lab
Department of Biomedical Engineering, Bucknell University, Lewisburg, PA

mbk018@bucknell.edu

Optimal Tissue Activation During Thalamic Deep Brain Stimulation for Essential Tremor

Keeler Thomas[1] , Karlo A. Malaga, Ph.D.[1]

1. Department of Biomedical Engineering, Bucknell University, Lewisburg, PA

Introduction

- Essential tremor (ET) is a neurological movement disorder that manifests in the hands
- ET affects 1% of the population, and 5% of people above 65 years [1]
- Deep brain stimulation (DBS) is a surgical option for ET patients to treat tremors
- Motor thalamus (VIM) is the traditional gray matter (GM) target for ET DBS (**Figure 1**)
- Side effects of ET DBS include paresthesia, dysarthria, and muscle contractions
- Recent studies suggest stimulating local white matter (WM) dentatorubrothalamic tract (DRT) [2]

Research Question: Is more WM tissue stimulation associated with therapeutic outcomes (tremor alleviation) or side effects (paresthesia, dysarthria, etc.)?

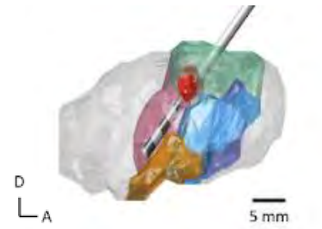

Figure 1. Visualization (sagittal view) of inactive electrodes (black) as well as active electrode and VTA (red) during VIM (blue) DBS for ET. [3]

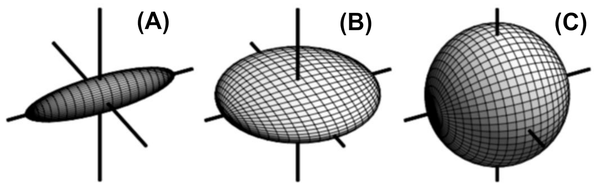

Figure 2. Glyphs representing (A) linear anisotropic diffusion, (B) planar diffusion, and (C) spherical isotropic diffusion. Linear anisotropic leads to high FA. Spherical isotropic leads to high MD. [4]

Methods

- 18 ET patients previously received unilateral VIM DBS; received DTI brain scans
- Volumes of tissue activation (VTAs) were previously modeled in COMSOL
- Calculated mean diffusivity (MD) and fractional anisotropy (FA) values (**Figure 2**)
  - MD = measure of total diffusion volume
  - FA = measure of diffusion bias in particular direction
- Implemented machine learning algorithms to classify voxels as cerebrospinal fluid (CSF), WM, and GM based on MD and FA values associated with each voxel
  - k-means classification algorithm clusters points based on input features
  - Support vector machine (SVM) classification algorithm trained on ground truth input features, then classifies new data based on learning scheme
- Calculated percent activation of various tissues (VIM, WM, etc.)
- Analyzed percent WM tissue activation and tremor outcome

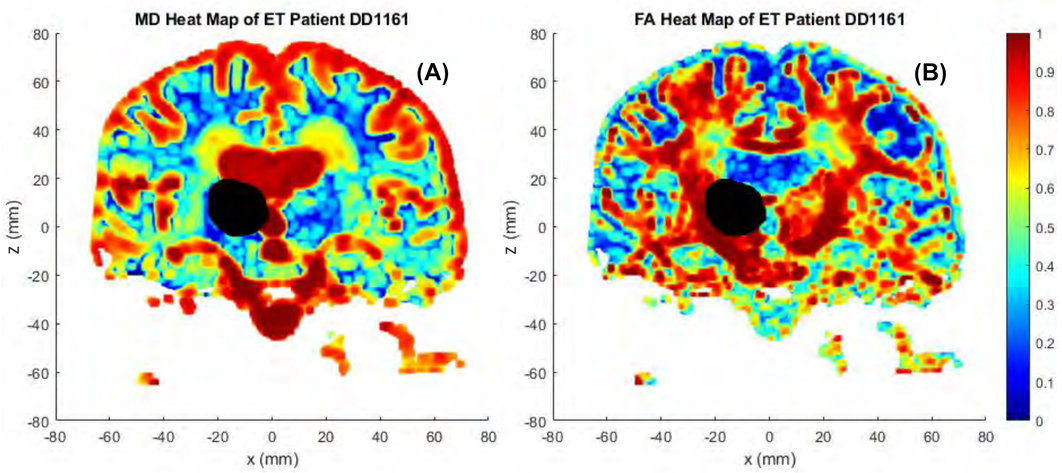

Figure 3. Heat maps of (A) mean diffusivity (MD) and (B) fractional anisotropy (FA) values (hotter = higher value) for exemplar ET patient DD1161. Ground truth thalamus plotted in black.

Results

Train and test machine learning algorithms on separate data

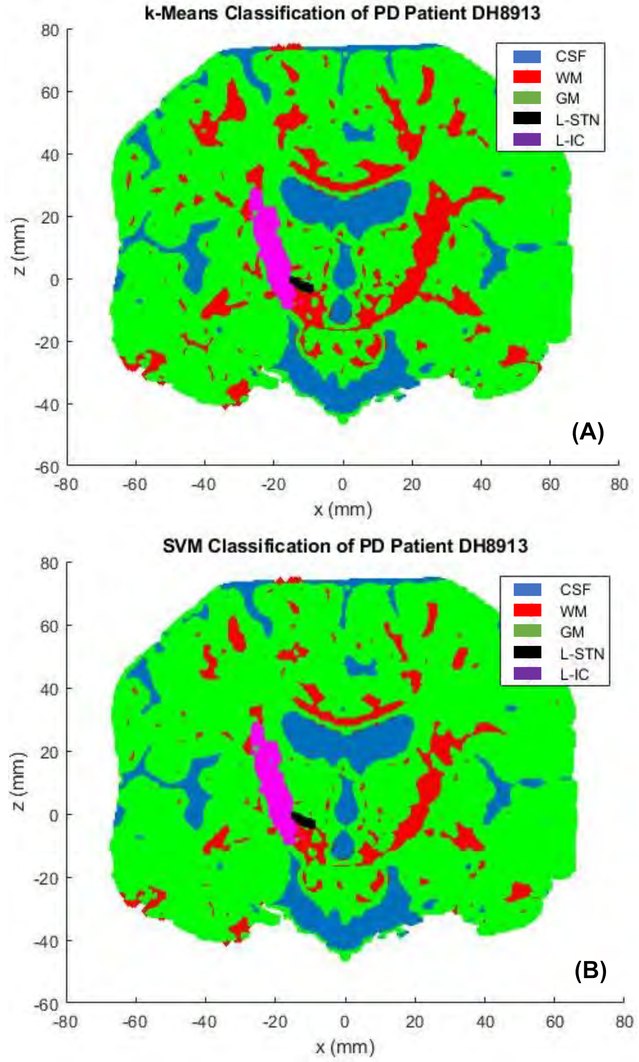

Figure 4. Tissue segmentation of exemplar Parkinson's disease patient DH8913. Coronal slice of tissue classified as CSF (blue), GM (green), and WM (red) with ground truth internal capsule (magenta) and subthalamic nucleus (black) plotted. (A) K-means classification had 92.9% WM and 41.0% GM accuracy. (B) Linear SVM classification had 78.6% WM and 60.6% GM accuracy. Quadratic SVM classification had 68.1% WM and 56.0% GM accuracy.

Table summary of classification algorithm accuracy

Table 1. Comparison of best machine learning algorithms and their white matter (WM) and gray matter (GM) percent accuracies.

	Algorithm		
	k-means	Linear SVM	Quadratic SVM
GM	41.0%	60.6%	56.0%
WM	92.9%	78.6%	68.1%

Equations for percent accuracy calculation

$$\text{WM accuracy (\%)} = \frac{Number\ of\ WM\ voxels\ in\ the\ IC}{Total\ number\ of\ IC\ voxels}\ x\ 100$$

$$\text{GM accuracy (\%)} = \frac{Number\ of\ GM\ voxels\ in\ the\ STN}{Total\ number\ of\ STN\ voxels}\ x\ 100$$

WM tissue activation is common among all therapeutic VTAs

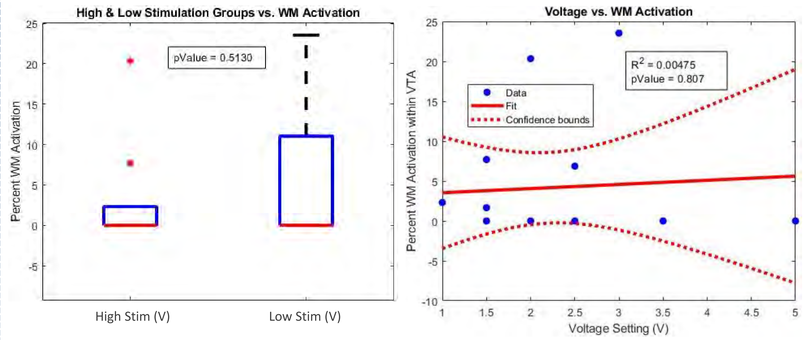

Figure 5. Boxplot and linear regression analyzing stimulation setting effect on WM tissue activation (n=15). High stimulation is from 2.5 V and above (n=5), low stimulation is below 2.5 V (n=10). No significance means therapeutic settings always involve some WM activation.

Equations for percent activation calculation

$$\text{WM activation (\%)} = \frac{Number\ of\ WM\ voxels\ in\ the\ VTA}{Total\ number\ of\ VTA\ voxels}\ x\ 100$$

$$\text{GM activation (\%)} = \frac{Number\ of\ GM\ voxels\ in\ the\ VTA}{Total\ number\ of\ VTA\ voxels}\ x\ 100$$

Conclusions

- Mean diffusivity and fractional anisotropy are effective metrics to segment CSF and WM respectively, with GM remaining; could explain the low accuracy when classifying GM voxels
- k-means clustering is more effective at classifying WM than support vector machines (linear, quadratic, etc.)
- WM is a common tissue type in therapeutic VTAs

Future Work

- Include all patient outcome VTAs
- Correlate individual patient outcomes (therapeutic vs. side-effect) as a function of WM tissue activation

Abbreviations

Essential tremor = ET
Deep brain stimulation = DBS
Ventral intermediate nucleus = VIM
Gray matter = GM
White matter = WM
Cerebrospinal fluid = CSF
Dentatorubrothalamic tract = DRT
Volume of tissue activation = VTA
Mean diffusivity = MD
Fractional anisotropy = FA
Support vector machine = SVM

References

1. Haubenberger, D., & Hallett, M. (2018). Essential Tremor. *New England Journal of Medicine*, *378*(19), 1802–1810.
2. Dembek, T. A., et. al (2020). PSA and VIM DBS efficiency in essential tremor depends on distance to the dentatorubrothalamic tract. *NeuroImage: Clinical*, *26*.
3. Malaga, K. A. (2019). *Finite Element Electrode and Individual Patient Modeling to Optimize Restorative Neuroengineering* (dissertation). *University of Michigan Library*. Retrieved from https://deepblue.lib.umich.edu/handle/2027.42/151626.
4. Zhang, S., Laidlaw, D. H., Kindlmann, G. (2005). Diffusion Tensor MRI Visualization. 327-340.
5. Elaff, I. (2016). Brain tissue classification based on diffusion tensor imaging: A comparative study between some clustering algorithms and their effect on different diffusion tensor imaging scalar indices. *Iranian Journal of Radiology*, *13*(2).

Acknowledgements

The authors would like to thank the patients involved in this study for their voluntary participation and Parag G. Patil, M.D., Ph.D., Kelvin L. Chou, M.D., Aidan Ahamparam, and Wutt Kyi from the University of Michigan for clinical data and data visualization code.

This projected was funded by the Program for Undergraduate Research at Bucknell University.

Contact Information

Computational Neuromodulation Lab
Department of Biomedical Engineering, Bucknell University, Lewisburg, PA

kpt004@bucknell.edu

Deep Brain Stimulation of the Subthalamic Nucleus and its Effect on Verbal Fluency in Parkinson Disease

Mary Robinson, Karlo A. Malaga, Ph.D.
Department of Biomedical Engineering, Bucknell University, Lewisburg, PA

Introduction

- Deep brain stimulation (DBS) is commonly used to treat the symptoms of Parkinson disease (PD). (tremor, rigidity, bradykinesia, and postural instability)
- DBS involves surgically implanted electrodes that stimulate structures deep in the brain with pulses of electricity controlled by a pacemaker.
- Volume of tissue activation (VTA) modeling is used to determine stimulation location
- A prevalent effect caused by DBS of the STN is the non-motor complications occurring in patients
- These non-motor complications include: verbal fluency (VF), fatigue, depression, and amnesia
- Semantic verbal fluency (SVF) - patients generate words in a category in a specified amount of time
- Phonemic verbal fluency (PVF) - patients generate words starting with a specific letter in a certain time frame

Objective: Identify the area of the STN that maximizes improvement in motor symptoms and minimizes the occurrence of non-motor side effects, specifically verbal fluency.

Methods

- 27 PD patients received STN DBS (Left STN n = 26, Right STN n = 27)
- VTA of the STN was calculated for each patient in the form of a percentage in the dorsal/ventral, lateral/medial, and anterior/posterior directions
- Both semantic and phonemic verbal fluency scores were collected before and after bilateral DBS
- Linear regression graphs were used to assess the relationship between lead location and VF outcomes
- Box Plots were used to assess the relationship between activation and VF outcomes
- Dorsal, lateral, and anterior directions were labeled as positive
- Ventral, medial, and posterior directions were labeled as negative
- Electrode location values were all normalized due to differences in STN sizes between patients

$$Normalization = \frac{Center\ of\ STN - Electrode\ location}{|STN\ Max - STN\ Min|}$$

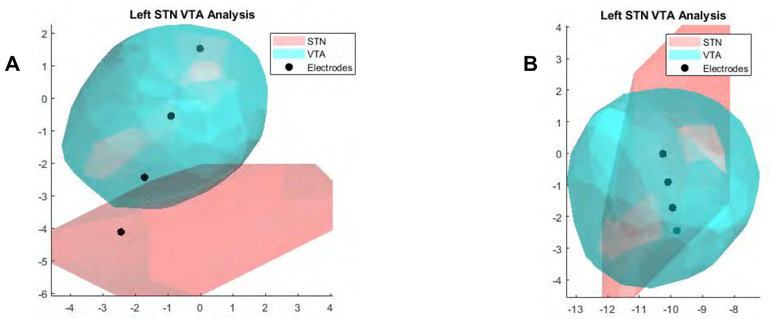

Figure 1. A. Sagittal view of VTA (blue), STN (red), and electrodes (black) B. Coronal view of VTA (blue), STN (red), and electrodes (black)

Results

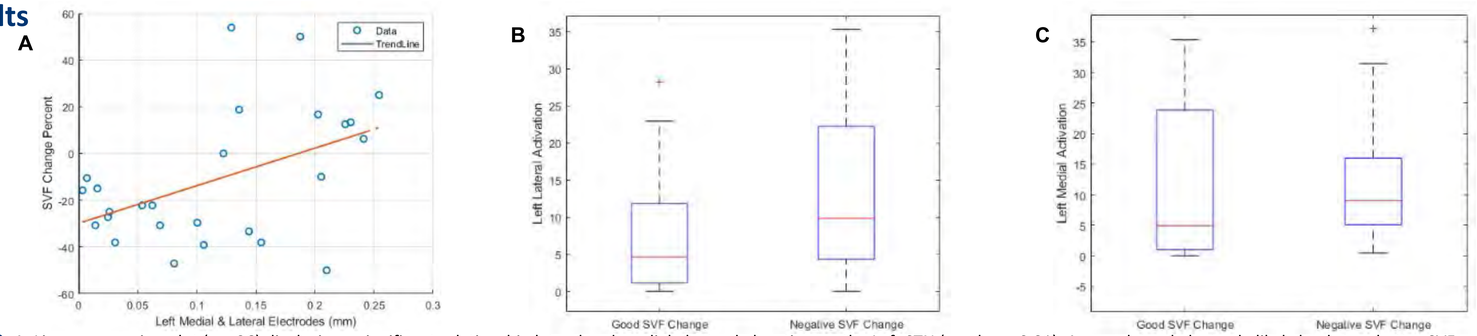

Figure 2. A. Linear regression plot (n = 26) displaying a significant relationship lateral and medial electrode location on the Left STN (p-value = 0.01). A more lateral electrode likely leads to a better SVF score B. Box plot comparing left STN lateral activation to SVF change C. Box plot comparing left STN medial activation to SVF change

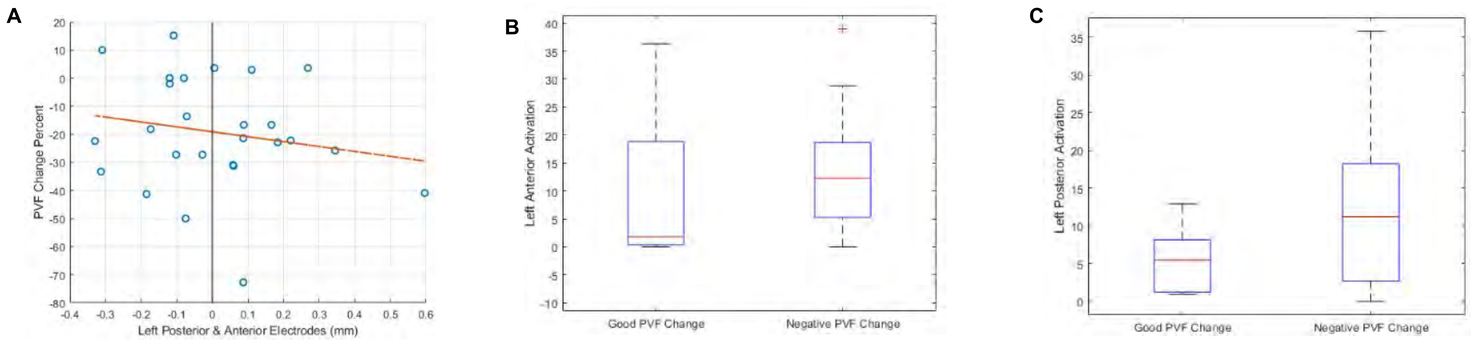

Figure 3. A. Linear regression graph shows as electrode location in the left STN becomes more anterior, PVF trends downward but is not statistically significant B.Box plot comparing left STN anterior activation to PVF change C. Box plot comparing left STN posterior activation to PVF change

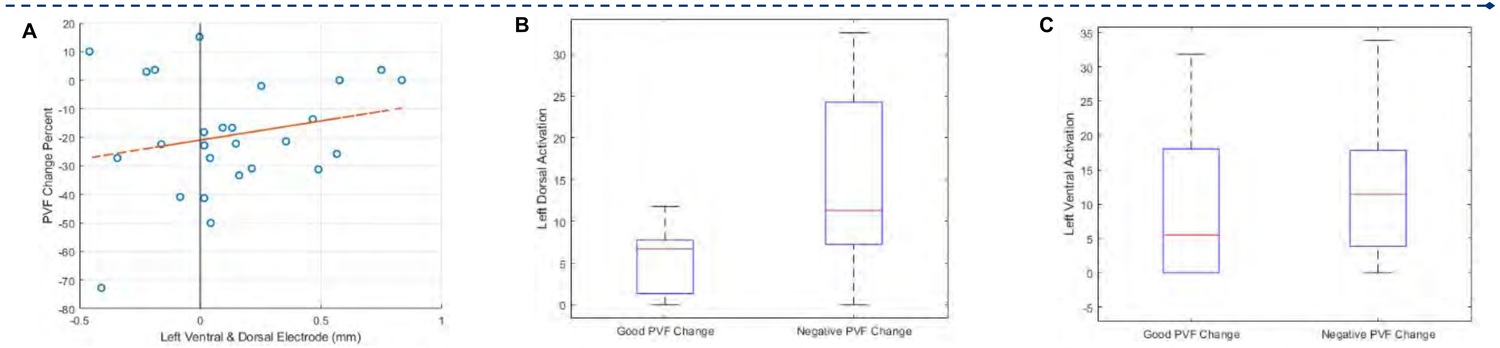

Figure 4. A. Linear regression graph (n = 26) shows as electrode location in the left STN becomes more Dorsal, PVF shows a greater negative effect B. Box plot comparing left STN dorsal activation to PVF change C. Box plot comparing left STN ventral activation to PVF change

Discussion

- There is a significant relationship between electrode location in the lateral section of the left STN and a reduction in SVF decline
- More posterior and dorsal electrode contact shows a trend in reduction in PVF decline
- Right STN DBS displays no significant correlation with VF decline
- Electrode location that is in the left anterior STN region shows a trend leading to a greater decline in PVF scores, but result is not statistically significant
- A greater amount of posterior activation in the left STN trends to a greater decline in PVF than anterior activation in the left STN but not statistically significant
- Electrode location does not equal VTA location

References

1.Greif, Taylor R., et al. "Anterior lead location predicts verbal fluency decline following STN-DBS in Parkinson's disease." Parkinsonism & Related Disorders 92 (2021): 36-40.
2. John, Kevin D., et al. "Deep brain stimulation effects on verbal fluency dissociated by target and active contact location." Annals of Clinical and Translational Neurology 8.3 (2021): 613-622.
3. Malaga, Karlo A., et al. "Atlas-independent, N-of-1 tissue activation modeling to map optimal regions of subthalamic deep brain stimulation for Parkinson disease." NeuroImage: Clinical 29 (2021): 102518.

Acknowledgements

The authors thank the patients involved in this study for their voluntary participation and Parag G. Patil, M.D., Ph.D., Kelvin L. Chou, M.D., Aidan Ahamparam, and Joseph T. Costello from the University of Michigan for clinical data and data visualization code.
This projected was funded by the Engineering Success Alliance Summer Research Scholarship at Bucknell University

Contact Information

Computational Neuromodulation Lab
Department of Biomedical Engineering, Bucknell University, Lewisburg, PA

mjr041@bucknell.edu

Accessing Stability of Thalamic Segmentation using Diffusion Tensor MRI

Rebecca Stinson, Karlo A. Malaga, Ph.D.

Department of Biomedical Engineering, Bucknell University, Lewisburg, PA

Introduction

- Essential Tremor is a neurological disorder characterized by shaking hands, head, or trunk.
- Essential Tremor is estimated to affect up to 7 million Americans [1]
- ET can be treated using deep brain stimulation (DBS) in which electrodes provide electrical stimulation to the thalamus
- DBS for ET targets the ventral intermediate thalamic nucleus (VIM) also called the ventral lateral thalamic nucleus, ventral part (VLpv) [2]
- Thalamus has no visual clues to the divisions between thalamic nuclei
- Algorithms based on diffusion tensor magnetic resonance imaging (dtMRI) aim to identify different thalamic nuclei to allow for patient-specific targeting during DBS.
- There are variations in the number of thalamic nuclei used in these algorithms

Objective

Identify the number of thalamic nuclei that produces the most stable segmentation of the thalamus.

Methods

- dtMRI collected from 22 patients undergoing DBS treatment for ET.
- A k-means algorithm was used to classifying each of the voxels within the thalamus as belonging to each nuclei.
- Algorithm accounted for the distance between the voxel and the nucleus centroid, as well as the similarity of the voxel's diffusion tensor values compared to the nucleus' average diffusion tensor.
- A set of 13 or 11 seeds were randomly placed within the thalamus and the algorithm was allowed to run until none of the centroids moved more than one millimeter between iterations.
- Each cluster of points was labelled using a linear pairing model comparing the segmentation to the Morel Atlas of the thalamus.
- The volume and centroid position for each nuclei was recorded for 100 iterations for each patient.

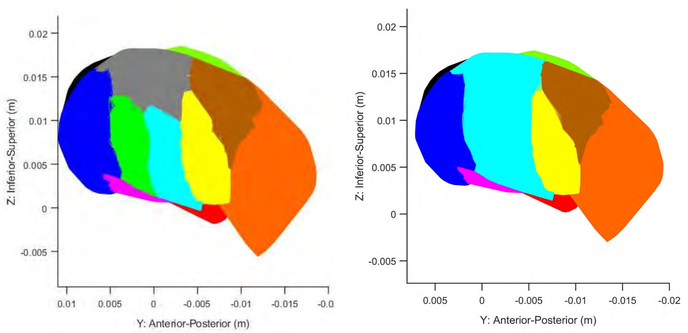

Figure 1: Atlas of the thalamus broken down into thirteen nuclei (left) and eleven nuclei (right) based on the Morel Atlas.
Key: Anterior (black), ventral anterior (blue), pulvinar (orange), ventral posterior lateral (yellow), ventral posterior medial (red), ventral medial (magenta), lateral posterior (brown), lateral dorsal (lime), ventral lateral anterior (green)*, ventral lateral-dorsal part (grey)*, ventral lateral-ventral part (cyan)*
*combined for 11-nuclei, represented as cyan
Not pictured: central median, medial dorsal

Results

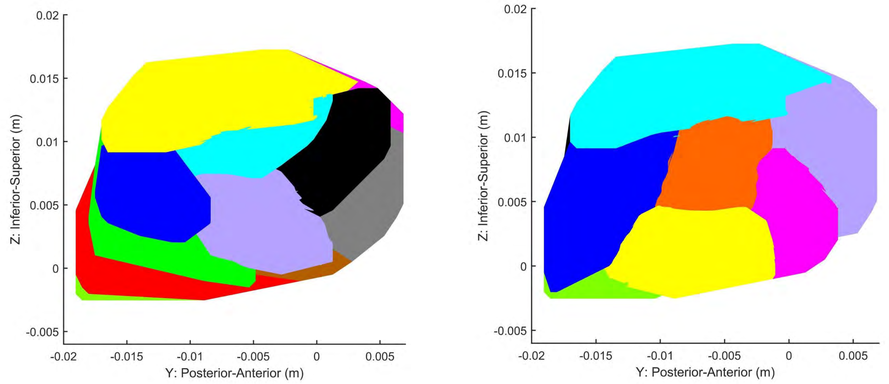

Figure 2: Sagittal view of the same subject's thalamus after being segmented into thirteen (left) and eleven (right) thalamic nuclei. The list of thirteen nuclei includes splitting the ventral lateral thalamic nucleus into ventral lateral anterior, ventral lateral dorsal part, and ventral lateral ventral part, while the list of eleven nuclei does not break the ventral lateral nucleus into subnuclei.

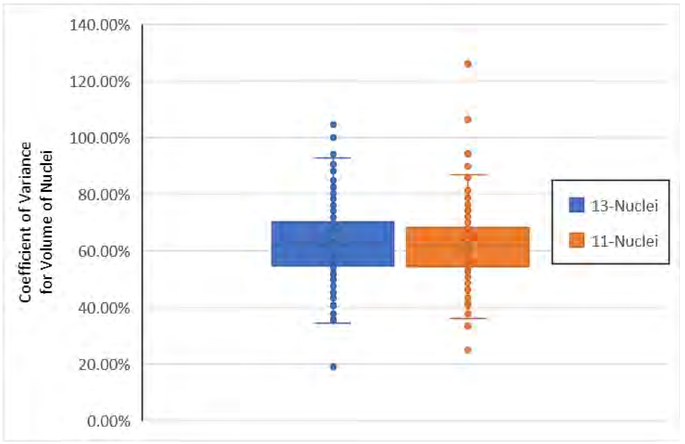

Figure 3: Coefficient of variance for the volume of each nucleus across 100 iterations. Both simulations had a large average coefficient of variance of 63% and 62% respectively.

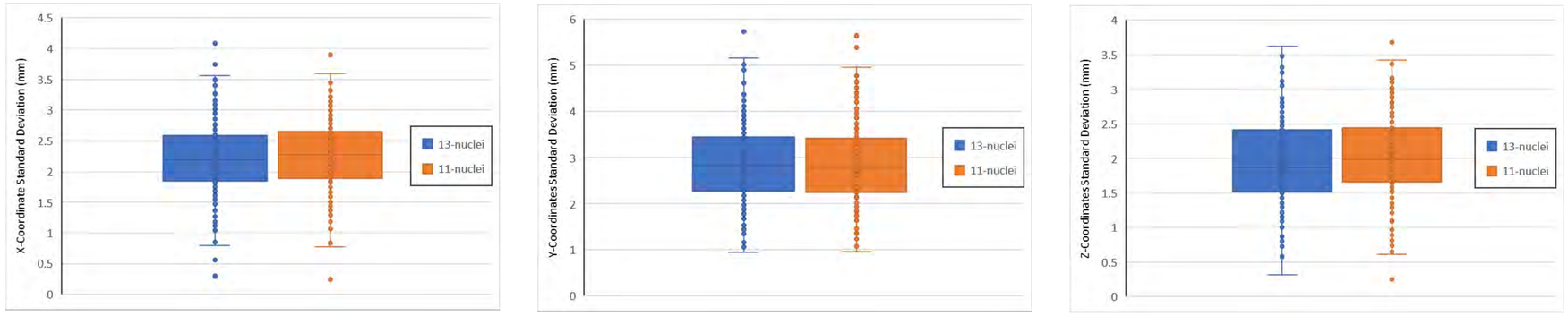

Figure 4: Standard deviation of centroid position for each nuclei across 100 iterations. Both thirteen and eleven nuclei simulations have a similar standard deviation indicating that the two models have a similar level of stability. The z-direction had the lowest variability with an average standard deviation of around 2 mm for both models. The y-direction had the most variability with an average standard deviation of around 2.85 mm for both models. The x-direction had an average standard deviation of 2.22mm and 2.28mm respectively.

Conclusion

Both numbers of nuclei used resulted in a large volume coefficient of variance. This suggests that both models are not stable as the volume of a given nucleus varies significantly across trials. Additionally, the centroid position has a standard deviation of more than 2 mm in all directions across the 100 trials. Ideally, the models would not vary significantly across trials so any run through of the segmentation would be representative of the algorithm. The variations could be in part due to the resolution of the MRI data as well as other noise causing the k-means algorithm to be inconsistent. If so, the model may become more stable at smaller numbers of nuclei.

Future Work

In the future, segmentations with 5, 7, 8, 10, and 12 nuclei will also be conducted and assessed for stability. Then the accuracy of each of the segmentations will be assessed. Accuracy will be determined based on comparing the areas of overlap between a patient's area of stimulation and the segmented nuclei with the reported side effects.

References

1. Louis, E. D., & Ottman, R. (2014). How Many People in the USA Have Essential Tremor? Deriving a Population Estimate Based on Epidemiological Data. Tremor and Other Hyperkinetic Movements, 4(0), 259. https://doi.org/10.7916/D8TT4P4B
2. Malaga, K. A., Houshmand, L., Costello, J. T., Chandrasekaran, J., Chou, K. L., & Patil, P. G. (n.d.). N-of-1 thalamic segmentation and tissue activation modeling in deep brain stimulation for essential tremor Running title: N-of-1 thalamic segmentation in DBS for ET.

Acknowledgements

The authors thank the patients involved in this study for their voluntary participation and Parag G. Patil, M.D., Ph.D., Kelvin L. Chou, M.D., Aidan Ahamparam, and Joseph T. Costello from the University of Michigan for clinical data and data visualization code.
This projected was funded by Bucknell University's Program for Undergraduate Research.

Contact Information
Computational Neuromodulation Lab
Department of Biomedical Engineering, Bucknell University, Lewisburg, PA

rjs062@bucknell.edu

Collecting Language Production Data Online

Jimmy Pronchick
Faculty Mentor: Heidi Lorimor
Bucknell University, Lewisburg, PA

Background

- **In English, people compute "agreement" on verb forms approximately every 12 words (or 5 seconds). (Eberhard, Cutting, & Bock, 2005)**
- **People sometimes make errors in verb forms.**

Agreement attraction:
Error resulting from a verb erroneously agreeing with features of a distractor noun:

Correct: *The gardener with the rakes **is** late.*
vs.
Attraction: *The gardener with the rakes **are** late.*

Vigliocco & Nicol (1998) argued that these errors happen, regardless of word order. Other work has shown that word order matters for sentence planning (Haskell & MacDonald, 2005).

Verb tense:
Verb tense errors result from the erroneous activation of the past tense form when the sentence requires a non-tensed form. The past tense form may be activated due to a parallel sentence planning or activation from other items in the sentence.

Correct: I didn't **buy** it - it was a gift.
vs.
Tense Error: I didn't **bought** it - it was a gift.

In our lab, we experimentally elicited verb tense errors using evidentials:

Sentence	Evidential	Completion
Christian ground coffee every morning.	He saw him.	"He saw him ground - oh god - grind coffee every morning."

Activation from other items:
- **Ground coffee** is a common noun phrase that contains the past participle of the required verb **grind**.
- **Ground** competes with **grind** and is coactivated due to the frequency of **ground coffee.**
- This may show parallel planning of structures happening during language production (Brehm, Cho, & Smolensky, 2022).

The Challenge

Pre-Covid, at Bucknell we ran language production studies in the Linguistics Lab (Coleman Hall).
- Participants sat at a computer
- We ran a script on a local computer that presented pictures/audio at particular times
- We recorded participants using a microphone

Now, running in-person experiments is more difficult.

The Goal

Create a way of conducting language production experiments online, which still allow us to collect audio data.

Experimental Setup

Participant recruitment:
- Prolific (www.prolific.co)

Experimental platform:
- Javascript (using libraries from jspysch.org)

Equipment:
- Participants use their own computers, with a microphone, and run the experiment in their web browser.
- The participant responses are downloaded to a Bucknell server.

Subject-verb agreement task
(replication of Vigliocco & Nicol, 1998)

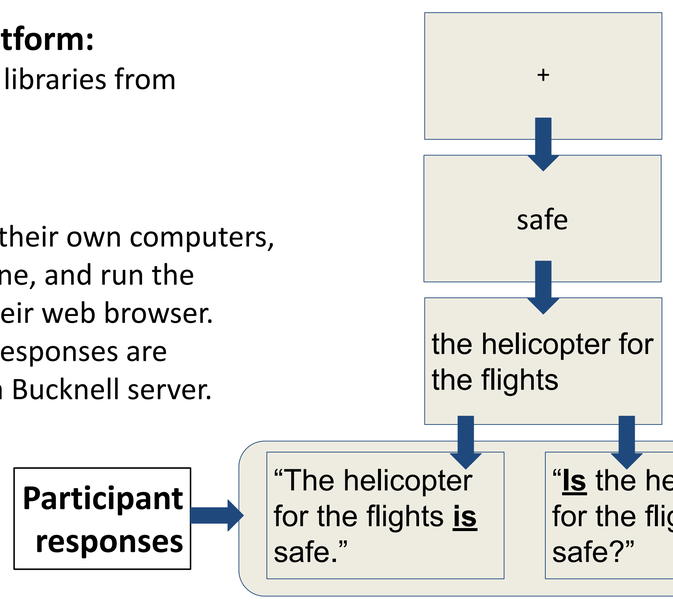

Q: Do you get the same pattern of errors for questions and statements?

Verb tense task

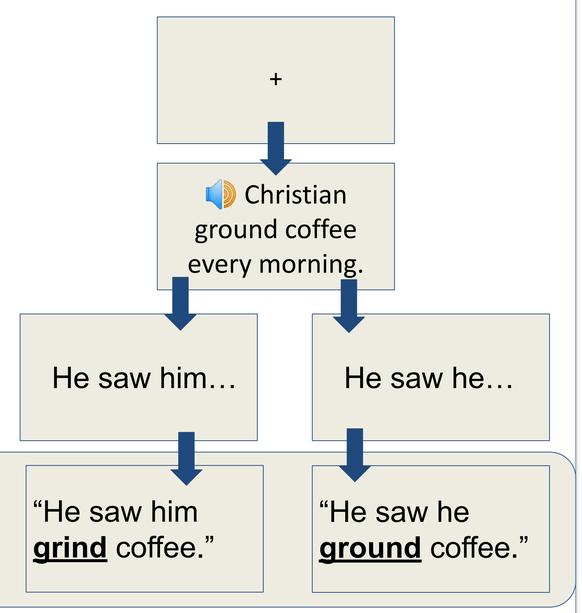

Qs: Can we elicit errors? Are the errors the same for "ground coffee" and "ground stone"?

Status of Experiments

Subject-verb agreement task
- We have run a pilot version of the Subject-verb agreement task and are preparing to release a full trial to ~120 participants.

Verb tense task
- We are finalizing the item sets for the Verb tense task, some possible past tense verb + noun combinations include:
  - scrambled eggs / scrambled images (e.g., "John scrambled eggs." : "She saw him scramble(d) eggs.")
  - spun wool / spun pinwheels
  - found objects / found worms

Discussion

Subject-verb agreement task
- If the results show that subject-verb number agreement errors pattern in questions than in statements, this would support the hypothesis that word order has an effect on language production (Haskell & MacDonald, 2005).

Verb tense task
- If the results from the verb tense task show a significantly higher error rate in sentences with common noun collocations, this would indicate that the parallel activation of other possible items plays a role in causing verb tense errors.

References

Brehm, Cho, & Smolensky. (2022). PIPS: A parallel planning model of sentence production. *Cognitive Science.*
Eberhard, Cutting, & Bock. (2005). Making syntax of sense: Number agreement in sentence production. *Psychological Review.*
Haskell & MacDonald (2005). Constituent structure and linear order in language production: Evidence from subject-verb agreement. *JEP: LMC.*
Vigliocco & Nicol. (1998). Separating hierarchical relations and word order in language production: Is proximity concord syntactic or linear? *Cognition.*